Indian winter and summer monsoon strength over the 4.2 ka BP event in foraminifer isotope records from the Indus River delta in the Arabian Sea

Alena Giesche[1], Michael Staubwasser[2], Cameron A. Petrie[3], and David A. Hodell[1]

[1] Godwin Laboratory for Palaeoclimate Research, Department of Earth Sciences, University of Cambridge, Cambridge, CB2 3EQ, United Kingdom
[2] Institute for Geology und Mineralogy, University of Cologne, Zülpicher Str. 49a, 50674 Cologne, Germany
[3] Department of Archaeology, University of Cambridge, Cambridge, CB2 3DZ, United Kingdom

Correspondence to: Alena Giesche (ag927@cam.ac.uk)

Abstract

The plains of northwest South Asia receive rainfall during both the Indian Summer (June-September) and Winter (December-March) Monsoon. Researchers have long attempted to deconstruct the influence of these precipitation regimes in paleoclimate records, in order to better understand regional climatic drivers and their potential impact on human populations. The Mid-Late Holocene transition between 5.3-3.3 ka BP is of particular interest in this region because it spans the period of the Indus Civilization from its early development, through its urbanization and onto eventual transformation into a rural society. An oxygen isotope record of the surface-dwelling planktonic foraminifer *Globigerinoides ruber* from the northeast Arabian Sea provided evidence for an abrupt decrease in rainfall and reduction in Indus River discharge at 4.2 ka BP, which the authors linked to the decline of the urban phase of the Indus Civilization (Staubwasser et al., 2003). Given the importance of this study, we used the same core (63KA) to measure the oxygen isotope profiles of two other foraminifer species at decadal resolution over the interval from 5.4 to 3.0 ka BP, and replicate a larger size fraction of *G. ruber* than measured previously. By selecting both thermocline-dwelling (*Neogloboquadrina dutertrei*) and shallow-dwelling (*Globigerinoides sacculifer*) species, we provide enhanced detail of the climatic changes that occurred over this crucial time interval. We found evidence for a period of increased surface water mixing, which we suggest was related to a strengthened winter monsoon with a peak intensity over 200 years from 4.5 to 4.3 ka BP. The time of greatest change occurred at 4.1 ka BP when both the summer and winter monsoon weakened, resulting in a reduction in rainfall in the Indus region. The earliest phase of the urban Mature Harappan period coincided with the period of inferred stronger winter monsoon between 4.5-4.3 ka BP, whereas the end of the urbanized phase occurred some time after the decrease in both the summer and winter monsoon strength by 4.1 ka BP. Our findings provide evidence that the initial growth of large Indus urban centers coincided with increased winter rainfall, whereas the contraction of urbanism and change in subsistence strategies followed a reduction in rainfall of both seasons.

1. Introduction

The ~4.2 ka BP event is considered to be a defining event of the Mid-Late Holocene transition period (Mayewski et al., 2004), and is marked by intense aridity in much of western Asia, which has been linked to cultural transitions in Mesopotamia, Egypt, and the Indus Civilization (Staubwasser and Weiss, 2006; Weiss, 2016). Recently, a climate reconstruction from Mawmluh cave in northeastern India has been used to formally demarcate the post-4.2 ka BP time as the Meghalayan Age (Letter from the 44th International Union of Geological Sciences, 2018; Walker et al., 2012). However, defining the exact timing and extent of aridity at ~4.2 ka BP remains an open question (Finné et al., 2011; Wanner et al., 2008). In this special issue devoted to the "4.2 ka event", we provide new paleoclimate data from a marine core in the northern Arabian Sea over this critical time interval to better understand the changes that occurred in both winter and summer hydroclimate over the Indian Subcontinent.

The $\delta^{18}O$ record of *Globigerinoides ruber* from marine core 63KA, obtained from the Arabian Sea off the coast of Pakistan and produced by Staubwasser et al. (2003), was among the first well-resolved paleoclimate records to suggest a link between a decrease in Indus River discharge around 4.2 ka BP and the decline of the urban phase of the Indus Civilization. Since the publication of this record, several other terrestrial paleoclimate reconstructions from the region (Berkelhammer et al., 2012; Dixit et al., 2014, 2018; Giosan et al., 2012; Kathayat et al., 2017; Menzel et al., 2014; Nakamura et al., 2016; Prasad and Enzel, 2006), and a number of marine reconstructions (Giosan et al., 2018; Gupta et al., 2003; Ponton et al., 2012) have added to our understanding of the complex relationship between the Indus Civilization and climate change. New questions have also emerged about the relative importance of winter rain from the Indian Winter Monsoon (IWM) system and summer rain from the Indian Summer Monsoon (ISM) during the critical time period from 5.4 to 3.0 ka BP, which spans the pre-urban, urban, and post-urban phases of the Indus Civilization (Giosan et al., 2018; Petrie et al., 2017; Prasad and Enzel, 2006). This is because the winter rain zone partially overlaps with the summer rain zone (Figure 1), and provides a critical supply of rain and snowfall for the Indus River basin. However, we currently understand much less about the behavior of the IWM than the ISM.

At its height, the Indus Civilization spanned a considerable geographical area with a greater extent than the other ancient civilizations of its time (Agrawal, 2007; Possehl, 2003). Today, the region that was once occupied by Indus populations is marked by a heterogeneous rainfall pattern, and some locations in the central Thar desert receive as little as 100 mm yr^{-1}, which is only about 10% of the amount of direct annual rainfall compared to New Delhi. Scarce direct precipitation in the central regions around the Thar Desert is supplemented in some cases by fluvial or groundwater sources. In addition, the distribution of winter rain (increasing towards the northwest) is distinct from summer rain (increasing towards the east), making regions variably suitable for growing certain crops and grazing (Petrie et al., 2017; Petrie and Bates, 2017). While many paleoclimate studies from South Asia (references A-C, I, K-M, S, and U in Figure 1) have theorized about the overall climatic impact of drought (and in most cases identified summer monsoon as the cause), it is important to identify changes in the relative contributions and timing of seasonal rainfall from both the winter and summer monsoons. Previously, it has not been possible to reliably differentiate winter and summer rain in reconstructions from the Indus region.

In this study, we re-examined the same marine core (63KA) used in the original research of Staubwasser et al. (2003). We first assessed the reproducibility of the *Globigerinoides ruber* $\delta^{18}O$ record using a larger size fraction of the same species for the time period 5.4-3.0 ka BP. We also measured the $\delta^{18}O$ of two additional foraminifer species, *G. sacculifer* (*Globigerinoides sacculifer*) and *N. dutertrei (Neogloboquadrina dutertrei)*, which live deeper than *G. ruber* in the water column. The different ecologies of the three species provide additional information with which to evaluate the multiple $\delta^{18}O$ records and assess seasonal changes in the paleoceanography of the northeastern Arabian Sea near the mouth of the Indus River.

The $\delta^{18}O$ of foraminifera has been widely applied as an indicator of temperature and salinity changes (Duplessy et al., 1992; Maslin et al., 1995; Wang et al., 1995; Rohling, 2000; among others). Measuring the $\delta^{18}O$ of species calcifying at different depths can provide further information about upper ocean seasonal hydrography such as surface water mixing, depth of the thermocline, and upwelling (Ravelo and Shackleton, 1995). Similar methods have been applied by several other studies (Billups et al., 1999; Cannariato and Ravelo, 1997; Norris, 1998; Steinke et al., 2010; Steph et al., 2009; among others), including a reconstruction of East Asian Winter Monsoon strength in the South China Sea (Tian et al., 2005). Here we apply a comparable method to samples from core 63KA in the northeastern Arabian Sea because surface waters at this location are influenced by freshwater discharge from the Indus River and direct precipitation during the summer monsoon months, whereas enhanced upper ocean mixing occurs during the winter monsoon. We hypothesized that our new measurements of $\delta^{18}O$ of *G. sacculifer* and *N. dutertrei* would allow us to track changes in upper ocean mixing. Weaker IWM winds are expected to result in a shorter duration and/or less intense upper ocean mixing, although how this signal is ultimately related to the amount or distribution of winter rainfall in the Indus River catchment has not been demonstrated conclusively. Dimri (2006) studied Western Disturbances for the time period 1958-1997, and noted that years of surplus winter precipitation are linked to significant heat loss over the northern Arabian Sea, which is mainly attributed to intensified westerly moisture flow and enhanced evaporation. Such conditions would promote deeper winter mixing, and provide a basis for relating thermocline depth with IWM intensity. By comparing the $\delta^{18}O$ of multiple species of foraminifera we seek to infer variations in the relative strengths of the summer and winter monsoons, and by comparing the 63KA record to other nearby marine and terrestrial records we evaluate the potential role that climate played in cultural transformation of the Indus Civilization.

2. Site Description

2.1 Monsoon – land-based processes

Today, most of the annual precipitation over northwest South Asia stems from the ISM, and occurs mainly between June and September. The pressure gradient between the low-pressure Tibetan Plateau and high-pressure Indian Ocean is accompanied by the ITCZ (Intertropical Convergence Zone) reaching its northward maximum in summer, which draws in moisture over the subcontinent via southwesterly winds from the Indian Ocean (Gadgil, 2003). The summer rainfall gradient increases from the central Thar Desert (as little as 100 mm direct summer rainfall per year) to the Himalaya mountains in the north (>1000 mm) and the Aravalli range to the west (>500 mm) (Figure 1b).

The IWM rain falls between December through March, and is mainly the result of atmospheric Western Disturbances (Dimri and Dash, 2012; Yadav et al., 2012) originating over the Mediterranean and Black Sea (Hatwar et al., 2005) that allow for moisture incursion from the Arabian Sea (Rangachary and Bandyopadhyay, 1987). During the IWM, the pressure gradient is reversed from the summer condition, allowing the passage of Western Disturbances when the ITCZ moves southward. As winter transitions to spring, predominantly northeasterly winds shift to westerly winds (Sirocko, 1991) that result in peak winter rainfall over the plains of northwest India in February and March. Anomalously cool, evaporative conditions over the northern Arabian Sea (promoting deeper winter mixing) also correlates with increased winter precipitation in the western Himalayas (Dimri, 2006). The winter rainfall gradient increases from the southern Thar Desert (<10 mm per year) up to the Himalayas in the northwest (>400 mm) (Figure 1c). Overall, the IWM contributes between roughly 10 to 50% of the total annual rainfall of northwest South Asia today.

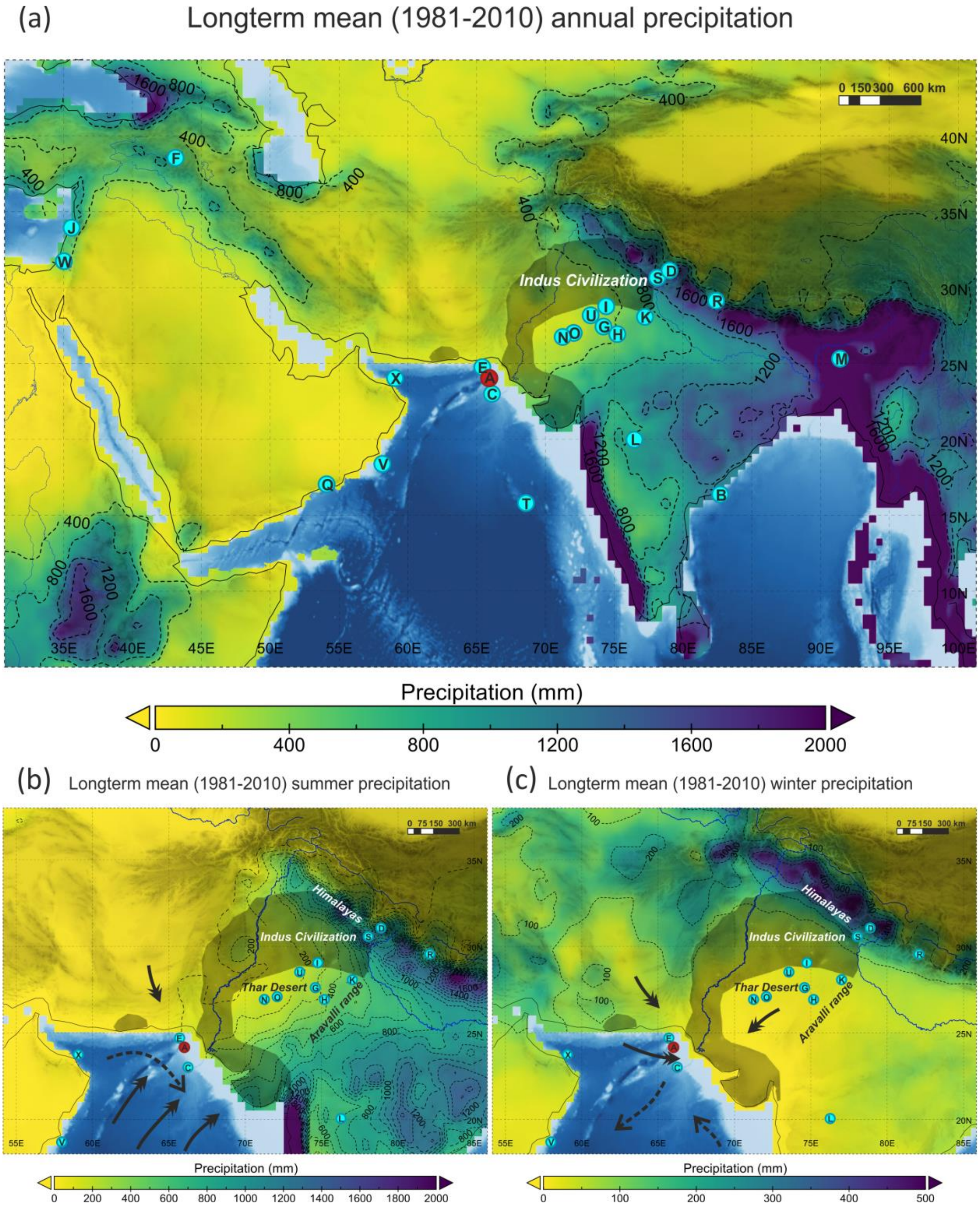

Figure 1. a. Annual **b.** ISM (JJAS) **c.** IWM (DJFM) mean precipitation (1981-2010) isohyets taken from the GPCC V7 global gridded dataset (0.5° x 0.5° resolution) (Schneider et al., 2015); note the difference in scale for summer and winter precipitation (0-2000 mm vs. 0-500 mm). Rainfall data overlain on GEBCO 2014 ocean bathymetry dataset (Weatherall et al., 2015), and shaded region shows extent of the Indus Civilization. Bold arrows show main wind directions, dashed arrows show ocean surface currents. Other studies discussed in this paper indicated by letters:

A Core 63KA – (this study; Staubwasser et al., 2003)
B Core 16A – (Ponton et al., 2012)
C Core Indus 11C – (Giosan et al., 2018)
D Din Gad peat record – (Phadtare, 2000)
E Core 39KG and 56KA – (Doose-Rolinkski et al., 2001)
F Lake Van record – (Wick et al., 2003; Lemcke and Sturm, 1997)
G Didwana playa lake – (Singh et al., 1990)

H Sambhar playa lake – (Sinha et al., 2006)
I Karsandi playa lake – (Dixit et al., 2018)
J Jeita cave speleothem – (Cheng et al., 2015)
K Kotla Dahar lake – (Dixit et al., 2014)
L Lonar lake – (Menzel et al., 2014)
M Mawmluh cave speleothem – (Berkelhammer et al.., 2012)
N Kanod playa lake – (Deotare et al., 2004)
O Bap Malar playa lake – (Deotare et al., 2004)
Q Qunf cave speleothem – (Fleitmann et al., 2003)
R Rara lake – (Nakamura et al., 2016)
S Sahiya cave speleothem – (Kathayat et al., 2017)
T Foraminifer trap EAST – (Curry et al., 1992)
U Lunkaransar playa lake – (Enzel et al., 1999)
V Core 723A, RC27-14, RC27-23, RC27-28 – (Gupta et al., 2003), (Overpeck et al., 1996)
W Soreq cave speleothem – (Bar-Matthews et al., 2003; Bar-Matthews and Ayalon, 2011)
X Core M5-422 – (Cullen et al., 2000)

The Indus and the other rivers that make up Punjab are partly fed by winter snow and ice melt from their upper mountain catchment areas. Melting peaks during the summer months around July-August (Yu et al., 2013), which coincides with the peak of ISM rainfall, and Indus River discharge reaches its maximum during August (Karim and Veizer, 2002). The proportion of winter to summer precipitation contributing to the Indus River is not entirely clear, although one study has estimated a 64-72% contribution of winter precipitation from the deuterium excess of Indus River water (Karim and Veizer, 2002), whereas a previous study estimated a lower 15-44% contribution of snowmelt to Indus tributaries (Ramasastri, 1999). Since the 1960s, the Indus River has seen more than a 50% reduction in discharge because of the construction of barrages as well as the diversion of water for agricultural uses (Ahmad et al., 2001).

2.2 Hydrography – core site and ocean-based processes

Core 63KA was obtained by the PAKOMIN cruise in 1993 (von Rad et al., 1995). The laminated core from the northeastern Arabian Sea (24° 37' N, 65° 59' E) was taken at 316 m water depth on the continental shelf, ~100 km west of the Indus River delta. The core has high sedimentation rates (equivalent to a temporal resolution of around 18 years/cm in the period of interest, 5.4-3.0 ka BP), and all foraminifer proxies were produced from the same laminated core with no bioturbation. An important aspect of core 63KA is that different components of the monsoon system are co-registered in the same sediment core, thereby permitting an explicit evaluation of the relative timing of different parts of the climate system (e.g., ISM and IWM).

Modern hydrographic conditions in the northeastern Arabian Sea are highly influenced by the seasonal monsoon. During summertime, highest sea surface temperatures (SSTs) are observed along with a shallow mixed layer depth <25 m (Schulz et al., 2002) (Figure 2a). A low salinity plume surrounds the Indus River delta and shoreline extending as far as the coring location (Supplemental Figure S1). The reverse occurs in winter when the lowest SSTs are accompanied by surface water mixing to >125 m, resulting in warming of the deeper waters (Schulz et al., 2002). Northeasterly winds promote convection in the northeastern Arabian Sea by cooling and evaporation of surface water (Banse, 1984; Madhupratap et al., 1996), and during the transition from winter to spring, wind directions shift from northeasterly to westerly (Sirocko, 1991).

The northern Arabian Sea is dominated by highly saline (up to 37 psu) surface waters known as Arabian Sea High Salinity Water (ASHSW), which extends from the surface down to 100 m depth (Joseph and Freeland, 2005). The high salinity is explained by the high evaporative rates over this region. ASHSW forms in the winter, but is prevented from reaching our coring site on the shelf by northerly subsurface currents until the summer (Kumar and Prasad, 1999). Along coastal areas, the ASHSW is starkly contrasted by the fresh water discharge of the Indus River, combined with direct precipitation. In contrast, surface waters in the Bay of Bengal on the eastern side of India have much lower surface water salinity, because of overall higher precipitation and stronger stratification from weaker winds (Shenoi et al., 2002). The heightened evaporative conditions and highly saline surface waters of the northeastern Arabian Sea make it a sensitive study location to observe changes in discharge of the entire Indus River catchment area – ultimately tracking changes in monsoon strength. Unlike individual terrestrial records, which may be affected by local climatic processes, the marine record from core 63KA is more likely to integrate regional changes of the large-scale ocean-atmosphere system.

Planktonic foraminifera complete their life cycle within a few weeks (Bé and Hutson, 1977). Peak abundances indicate the time of year when each species tends to calcify, thereby recording the $\delta^{18}O$ and temperature of the seawater in their $CaCO_3$ shells primarily during certain seasons. Foraminifer abundances in the eastern Arabian Sea have been studied by Curry et al. (1992) using sediment traps deployed at shallow (~1400 m) and deep (~2800 m) water depths ("T" in Figure 1a). *G. ruber* and *G. sacculifer* have peak abundances during the summer months (June-September), whereas *N. dutertrei* lives mainly during the winter and has a secondary peak in summer months (Figure 2c). Preferred depth ranges for each species reflect their ecological niches, including requirements for nutrients and tolerance for ranges of temperature and salinity (Bé and Hutson, 1977; Hemleben et al., 2012). *G. ruber* lives in the upper surface waters (0-10 m), *G. sacculifer* is found in slightly deeper surface waters (10-40 m), and *N. dutertrei* inhabits the base of the mixed layer near the thermocline (40-140 m) (estimates based on ranges from Farmer et al. (2007) and the local CTD profiles) (Figure 2d).

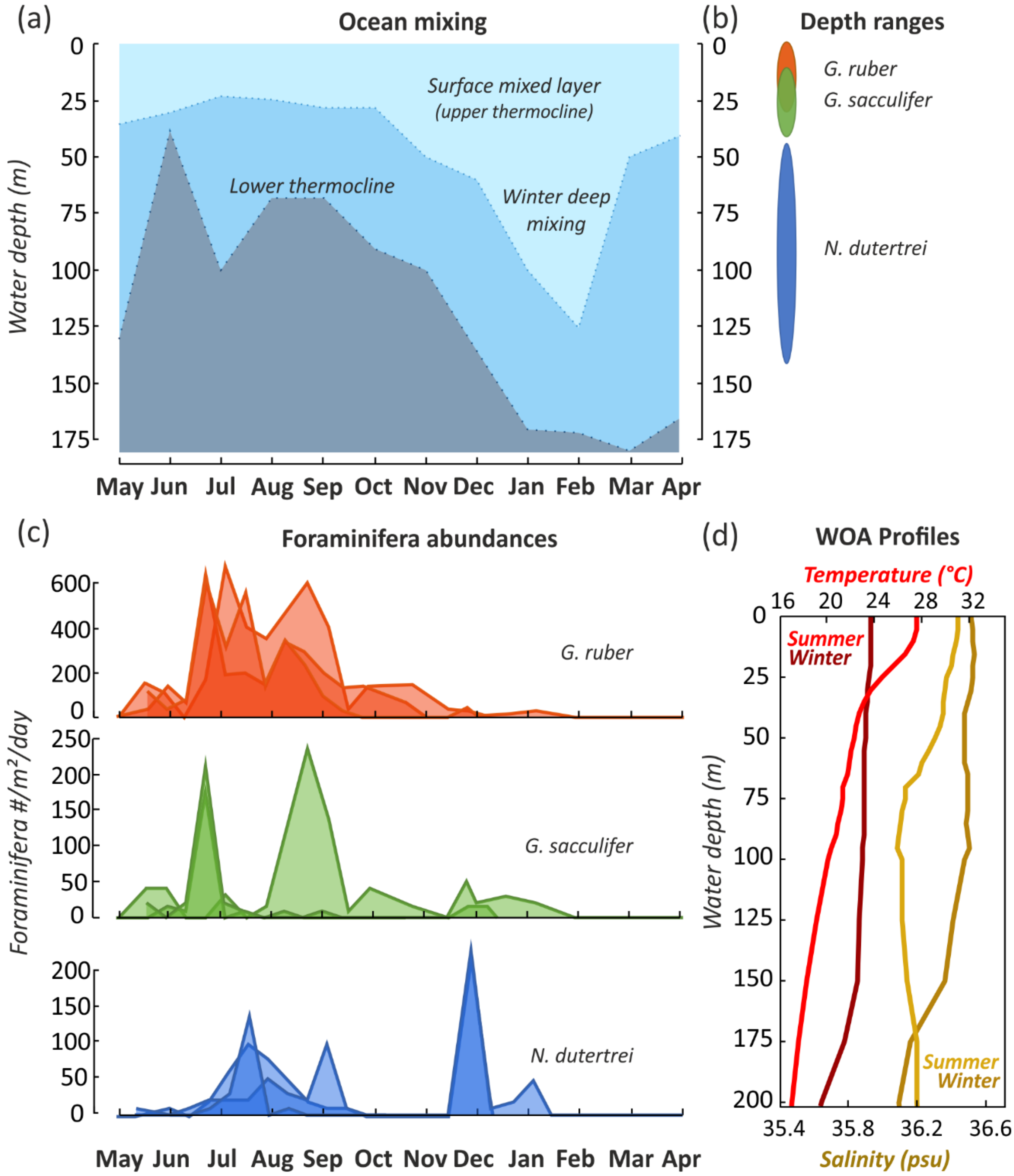

Figure 2. a. Seasonal surface water mixing depth based on station EPT-2 located nearby the coring site of 63KA (adapted from Schulz et al., 2002 who also used data from Hastenrath and Lamb, 1979) **b.** Foraminifer depth ranges based on CTD profile **c.** Foraminifer abundances from EAST traps (overlapping peaks indicate data from multiple traps): *G. ruber* (orange), *G. sacculifer* (green), and *N. dutertrei* (blue) (adapted from Curry et al., 1992 using Zaric, 2005) **d.** World Ocean Atlas (WOA) mean (1955-2012) temperature (red) and salinity (yellow) profiles at 24.875°N, 65.875°E, shown for summer (JAS) and winter (JFM) seasons (Locarnini et al., 2013; Zweng et al., 2013).

3. Materials and Methods

3.1 Age model

The radiocarbon dates from Staubwasser et al. (2002, 2003) were obtained from 80 samples of mainly the foraminifer *G. sacculifer* and three samples of *O. universa*. In the interval of interest (5.4-3.0 ka BP), there are 15 radiocarbon dates with a 95% confidence range of 30-130 years. The average sample resolution is 18 years/cm. Bayesian age modelling software, BACON v2.3.3 (Blaauw and Christen, 2011), was used as an R-package to update the age model of core 63KA. No major difference exists between the old and new age models, except for the period 13-11 ka BP (Supplemental Figure S5, Table S2). IntCal13 was used for radiocarbon calibration (Reimer et al., 2013) with marine reservoir ages provided by Staubwasser et al. (2002, 2003).

3.2 Stable isotope analysis

Oxygen and carbon isotopes were measured on three species of foraminifera selected from washed samples at 1-cm intervals throughout 132 cm of the core covering 5.4-3.0 ka BP: *G. ruber* (white, *sensu stricto*), *G. sacculifer*, and *N. dutertrei*. For *G. ruber*, 12 ± 8 foraminifera were picked from the 400-500µm size fraction with an average weight of 21.4 ± 2.5µg. The 400-500µm size fraction was picked because too few specimens remained in the size fraction 315-400µm used by Staubwasser et al. (2003). For *G. sacculifer*, 34 ± 7 foraminifera were picked from the 315-400µm size fraction with an average weight of 21.9 ± 2.6µg. For *N. dutertrei*, 34 ± 4 foraminifera were picked from the 315-400µm size fraction with an average weight of 25.9 ± 2.2µg. At some depth levels in the core there were insufficient foraminifera for measurement, along with outlier measurements in two cases, leaving 14 gaps in the *G. ruber* 400-500µm record, 4 gaps in the *G. sacculifer* record, and no gaps for *N. dutertrei*. The published *G. ruber* is from the 315-400µm size fraction and contains 17 gaps in the depth range examined (Staubwasser et al., 2003).

All foraminifera were weighed, crushed, and dried at 50° C. Samples were cleaned for 30 minutes with 3% H_2O_2, followed by a few drops of acetone, ultrasonication, and drying overnight. Where sample weights exceeded 80µg, oxygen and carbon isotopes were measured using a Micromass Multicarb Sample Preparation System attached to a VG SIRA Mass Spectrometer. In cases of smaller sample sizes, the Thermo Scientific Kiel device attached to a Thermo Scientific MAT253 Mass Spectrometer was used in dual inlet mode. This method adds 100% H_3PO_4 to the $CaCO_3$, water is removed cryogenically, and the dry CO_2 is analyzed isotopically by comparison with a laboratory reference gas. For both measurement methods, 10 reference carbonates and 2 control samples were included with every 30 samples. Results are reported relative to VPDB, and long-term reproducibility of laboratory standards (e.g., Carrara marble) is better than ±0.08‰ for $\delta^{18}O$ and ±0.06‰ for $\delta^{13}C$. Reproducibility of foraminiferal measurements was estimated by five triplicate (three separately picked) measurements of *G. ruber* (400-500µm) that yielded one standard deviation of ±0.12‰ ($\delta^{18}O$) and ±0.10‰ ($\delta^{13}C$). For *G. sacculifer* (315-400µm) the standard deviation of eight triplicate measurements was ±0.07‰ ($\delta^{18}O$) and ±0.07‰ ($\delta^{13}C$), and for *N. dutertrei* (315-400µm) the standard deviation of nine triplicate measurements was ±0.06‰ ($\delta^{18}O$) and ±0.07‰ ($\delta^{13}C$).

To calculate equilibrium values of $\delta^{18}O_{calcite(PDB)}$, we used the CTD profile from station 11 (24.62° N, 66.07° E) taken in September 1993 during PAKOMIN *Sonne* cruise no. 90 (von Rad, 2013), which is nearly identical to the location of core 63KA (24.62° N 65.98° E). The

$\delta^{18}O_{water(SMOW)}$ was calculated from salinity following Dahl and Oppo (2006), and $\delta^{18}O_{calcite(SMOW)}$ was further calculated using the calcite-water equation of Kim and O'Neil (1997). We also used the equation of Shackleton (1974) as a comparative method for calculating $\delta^{18}O_{calcite(PDB)}$.

3.3 Statistical treatment

Statistical tests were applied to the raw data from the $\delta^{18}O$ and $\delta^{13}C$ time series, including the package SiZer (Chaudhuri and Marron, 1999; Sonderegger et al., 2009) in R software (2016) that calculates whether the derivative of a time series exhibits significant changes given a range of timespans. A Pearson's correlation test (confidence level 95%) was done on paired samples from both size fractions of *G. ruber*. We also conducted a Welch's t-test to determine if the mean population of $\delta^{18}O$ is significantly different before and after 4.1 ka BP.

As in the original data of Staubwasser et al. (2003), the oxygen isotope results show great variability and distinguishing long-term trends in these data benefits from smoothing for visualization purposes. After completing all statistical tests and performing the differences on the raw data (132 depths), a loess (locally weighted) smoothing function was applied to the $\delta^{18}O$ and $\delta^{13}C$ data from 5.4-3.0 ka BP, using a 210-year moving window as described by Staubwasser et al. (2003). Loess smoothing uses weighted least squares, which places more importance on the data points closest to the center of the smoothing interval. The bandwidth of 210 years was considered a reasonable time window for capturing the overall trends in the dataset (other time windows are shown for comparison in Supplemental Figure S2).

4. Results

The new $\delta^{18}O$ measurements of *G. ruber* (400-500µm) parallel the published record of *G. ruber* (315-400µm) (Staubwasser et al., 2003), but the $\delta^{18}O$ of the specimens from the larger size fraction is offset by -0.23‰ on average (Figure 3). The records from two size fractions, produced in different laboratories by different investigators, display a weak positive correlation for the raw data ($R = 0.25$, $p < 0.01$, $n = 109$, slope 0.26, intercept -1.36), and the 210-year smoothed records reveal good agreement in the overall trends of the data. When comparing the two *G. ruber* records, it is apparent that the increasing trend in $\delta^{18}O$ starts well before ~4.2 ka BP – perhaps as early as ~4.9 ka BP. This trend is also observed with the SiZer analysis, which identifies a significant increase in $\delta^{18}O$ anywhere from 4.9 to 4.2 ka BP depending on which smoothing window is selected (Figure 4). The new $\delta^{18}O$ record of *G. ruber (*400-500µm) shows additional detail after the ~4.2 ka BP event – i.e. specifically, a double-peak maximum occurring at 4.1 and 3.95 ka BP that is related to seven discrete measurements with high $\delta^{18}O$ values. These maxima are offset from the average $\delta^{18}O$ value by +0.18‰ (smoothed average), or up to +0.38‰ when considering the maximum individual measurement at 4.1 ka BP. The offsets from the average values exceed one standard deviation of the entire record from 5.4-3.0 ka BP, which is 0.13‰. Although *G. ruber* shows an event at 4.1 ka BP, it does not show a permanent step change: A Welch's t-test comparing the means of pre- and post-4.1 ka BP indicates that the +0.07‰ shift in mean $\delta^{18}O$ values of *G. ruber* (315-400µm) is statistically significant (t value = 2.9, $p < 0.01$, $n = 115$), but the +0.03‰ shift in mean $\delta^{18}O$ values of *G. ruber* (400-500µm) is not significant (t value = 1.5, $p < 0.2$, $n = 118$).

393

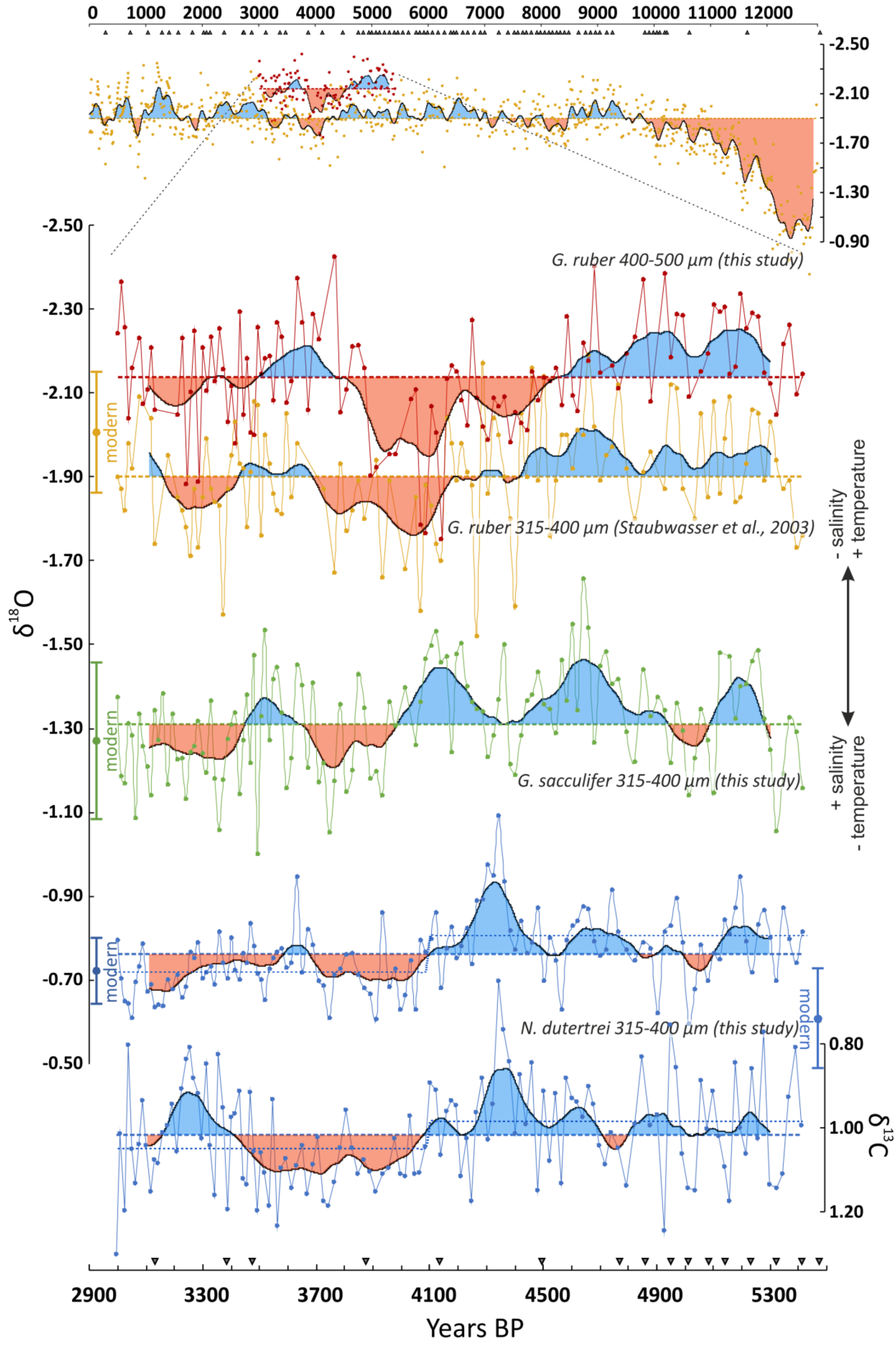

0
1000
2000
3000
4000
5000
6000
7000
8000
9000
10000
11000
12000
-2.50
-2.10
-1.70
-1.30
-0.90
G. ruber 400-500 µm (this study)
-2.50
-2.30
-2.10
-1.90
-1.70
-1.50
-1.30
-1.10
-0.90
-0.70
-0.50
δ18O
modern
modern
modern
modern
G. ruber 315-400 µm (Staubwasser et al., 2003)
G. sacculifer 315-400 µm (this study)
N. dutertrei 315-400 µm (this study)
- salinity
+ temperature
+ salinity
- temperature
0.80
1.00
1.20
δ13C
2900
3300
3700
4100
4500
4900
5300
Years BP

394

Figure 3. Core 63KA δ^{18}O *G. ruber* from two size fractions: 400-500µm (red) (this study), 315-400µm (orange) (Staubwasser et al., 2003), shown in the context of the original record and also zoomed in over 5.4-3.0 ka BP. δ^{18}O of *G. sacculifer* 315-400µm (green), and δ^{18}O and δ^{13}C of *N. dutertrei* 315-400µm (blue) are shown over the interval 5.4-3.0 ka BP. Data are shown with a 210-year loess smoothing, and modern surface values ±1σ are plotted for comparison. Mean values for all species are denoted by the dotted line, and the pre- and post-4.1 ka BP mean values are indicated by an additional dotted line for *N. dutertrei*. Individual AMS radiocarbon dates are denoted by triangles near the timeline.

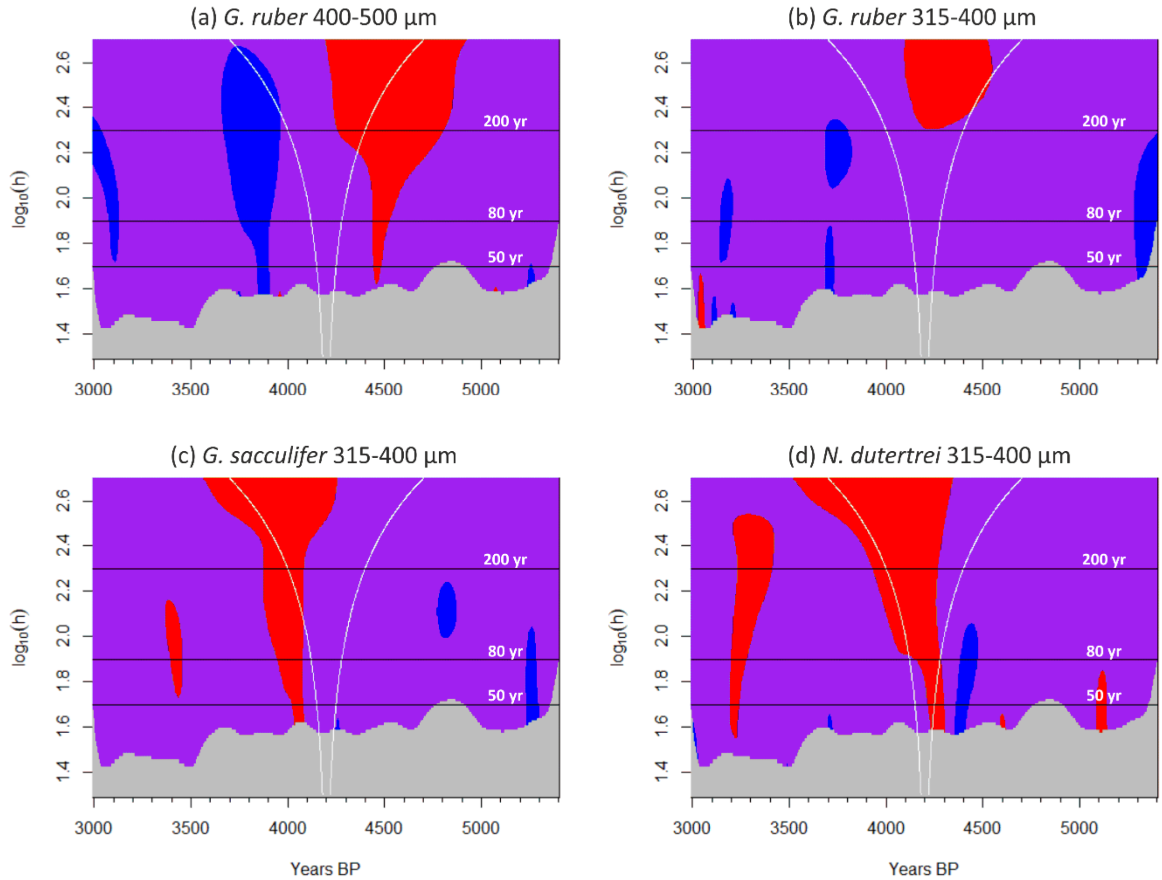

Figure 4. SiZer 1st derivative analysis (Chaudhuri and Marron, 1999; Sonderegger et al., 2009) applied to δ^{18}O of **a.** *G. ruber* 400-500µm, **b.** *G. ruber* 315-400µm, **c.** *G. sacculifer* 315-400µm, **d.** *N. dutertrei* 315-400µm. The red areas indicate statistically significant increases in δ^{18}O, the blue represent decreases, and the purple no significant change. Black horizontal lines are the smoothing bandwidths (h = 50, 80, and 200 years). The distance between the white lines denotes the change in smoothing bandwidth scaled to the x-axis.

The relative differences in δ^{18}O of the planktonic species studied (*G. ruber*, *G. sacculifer* and *N. dutertrei*) reflect the temperature and salinity of their habitat in the water column: δ^{18}O *G. ruber* < δ^{18}O *G. sacculifer* < δ^{18}O *N. dutertrei* (Figure 3). *G. sacculifer* is offset from *G. ruber* (315-400µm) by approximately +0.57‰, whereas *N. dutertrei* is offset by +1.14‰. The larger size fraction of *G. ruber* (400-500µm) is offset from *G. ruber* (315-400µm) by -0.23‰. The offsets among species are maintained throughout the entire record (Figure 3). We also measured δ^{18}O values near the top of the core (approximately the last 200 years) for all three species in the 315-400µm size fraction, which continue to show the same offsets

(Supplemental Figure S3). The $\delta^{18}O$ of *G. ruber* shows the greatest variance and *N. dutertrei* shows the least (Supplemental Figure S4, Table S1).

Equilibrium calcite calculations based on the salinity and temperature measurements from the September 1993 CTD profile of station 11 of the PAKOMIN Cruise (von Rad, 2013) show the expected depth habitats of the three foraminifer species (Figure 5). *G. ruber* is generally found at 0-30 m, *G. sacculifer* at 15-40 m, and *N. dutertrei* at 60-150 m (Farmer et al., 2007). Using the CTD profile from our core location, we compare these depth ranges with the measured $\delta^{18}O$ values. The calculated depths ranges agree well with those expected on the basis of other studies, placing *G. ruber* in the upper 10 m, *G. sacculifer* 10-40 m, and *N. dutertrei* 40-140 m.

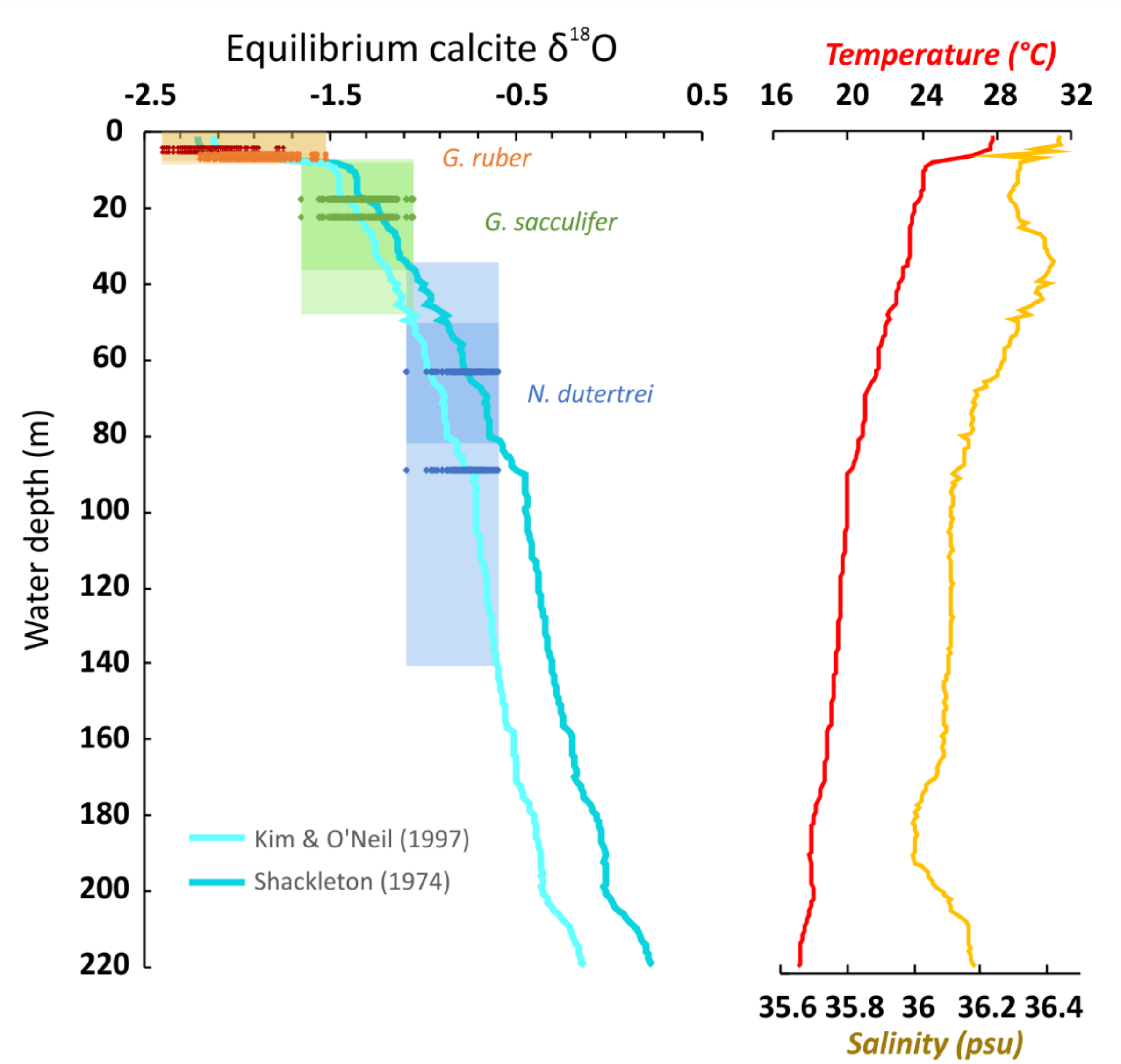

Figure 5. $\delta^{18}O$ of equilibrium calcite (left) calculated from the CTD temperature and salinity profile at station 11 (von Rad, 2013) (right) with projected depth ranges of *G. ruber* 400-500µm (red), *G. ruber* 315-400µm (orange), *G. sacculifer* 315-400µm (green), *N. dutertrei* 315-400µm (blue). We show estimated values using both the original paleotemperature equation of Shackleton (1974) (dark teal), and Kim & O'Neil (1997) (turquoise). Horizontal ranges show the measured $\delta^{18}O$ values of each species between 5.4-3.0 ka BP.

G. sacculifer $\delta^{18}O$ increases around 4.1 ka BP, and a Welch's t-test comparing the means of pre- and post-4.1 ka BP indicates that the +0.08‰ shift in mean $\delta^{18}O$ values is statistically significant (t value = 3.8, $p < 0.01$, n = 128). SiZer analysis also points to a statistically significant increase at ~4.1-3.9 ka BP, when considering all smoothing time windows between 20 and 500 years (Figure 4).

Likewise, the dominant change in the $\delta^{18}O$ of *N. dutertrei* is a mean increase at 4.1 ka BP (Figure 3). SiZer analysis also identifies a significant decrease in $\delta^{18}O$ occurring mainly between 4.45 and 4.35 ka BP, followed by a significant increase between 4.3 and 4.1 ka BP (Figure 4). A Welch's t-test comparing the means of pre- and post-4.1 ka BP indicates that the +0.08‰ shift in mean $\delta^{18}O$ values is statistically significant (t value = 6.2, $p < 0.01$, n = 132), along with the +0.07‰ shift in mean $\delta^{13}C$ (t value = 3.3, $p < 0.01$, n = 132).

Differencing $\delta^{18}O$ of foraminifera (expressed as $\Delta\delta^{18}O$) in the same sample can better emphasize signals of interest (Figure 6). The $\Delta\delta^{18}O$ of *G. ruber* 400-500µm and *G. ruber* 315-400µm size fractions shows increasing similarity between ~4.8 and 3.9 ka BP during the period of overall higher $\delta^{18}O$. The $\Delta\delta^{18}O$ of *N. dutertrei* and both size fractions of *G. ruber*, designated $\Delta\delta^{18}O_{d-r}$, reveals a period of more similar values between ~4.5 and 3.9 ka BP, with two minima at 4.3 and 4.1 ka BP. The $\Delta\delta^{18}O$ of *G. sacculifer* and both size fractions of *G. ruber* ($\Delta\delta^{18}O_{s-r}$) show a period of similar values between 4.3 and 3.9 ka BP, with a minimum difference at 4.1 ka BP. In contrast, the $\Delta\delta^{18}O$ of *N. dutertrei* and *G. sacculifer* ($\Delta\delta^{18}O_{d-s}$) shows the most similarity between 4.5 and 4.2 ka BP with a minimum at 4.3 ka BP, followed by the maximum differences between 4.2 and 3.9 ka BP that peaks at 4.1 ka BP.

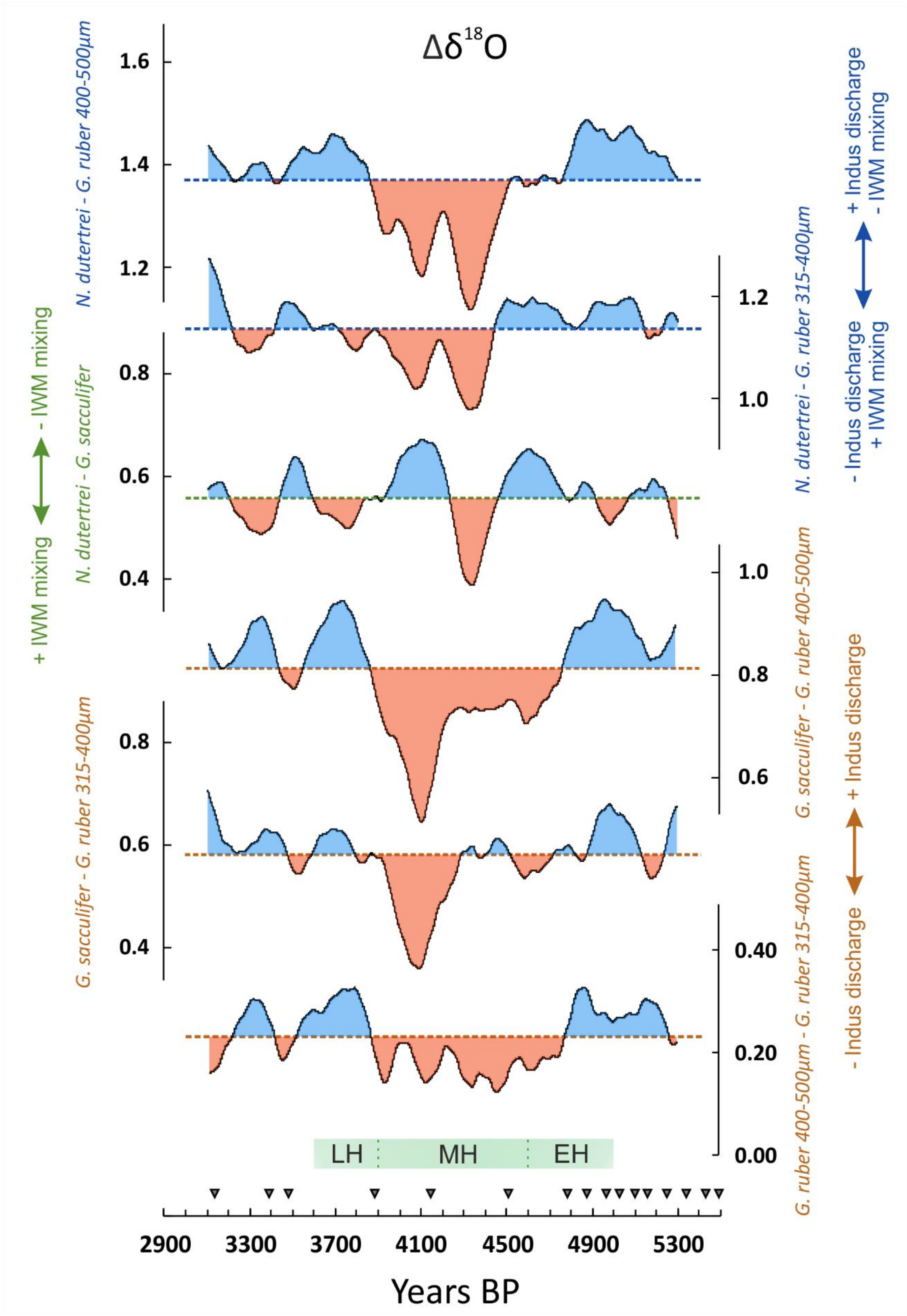

Figure 6. Core 63KA $\Delta\delta^{18}O$ shown with a 210-year loess smoothing. Individual AMS radiocarbon dates are denoted by triangles near the timeline. *G. ruber* 315-400µm size fraction data come from Staubwasser et al. (2003). The green band near the timeline showing EH, MH, and LH refers to Early Harappan (~5.0-4.6 ka BP), Mature Harappan (~4.6-3.9 ka BP), and Late Harappan (~3.9-3.6 ka BP) periods, respectively.

5. Discussion

5.1 Interpretation of foraminifer $\delta^{18}O$

The trends in the original $\delta^{18}O$ record of *G. ruber* (315-400µm) by Staubwasser et al. (2003) is reflected by our independent $\delta^{18}O$ measurements of *G. ruber* in a larger size fraction (400-500µm), although an important difference exists suggesting a decrease in freshwater discharge as early as 4.8 ka BP. The larger size fraction is offset by approximately -0.2‰, which is similar to the size-related fractionation of -0.3‰ per +100µm for *G. ruber* reported by Cayre and Bassinot (1998), and could be attributed to size-related vital effects. Alternatively, part of the offset might be explained by interlaboratory calibration considering the data were produced using two different methods and mass spectrometers.

The observed 4.1 ka BP maximum in $\delta^{18}O$ of *G. ruber*, living near the surface during summer months, could be attributed to either decreased SST or increased surface water salinity (Bemis et al., 1998). Staubwasser et al. (2003) acknowledged that a decrease in SST could cause the increase in $\delta^{18}O$ in the *G. ruber* record, but argued that this explanation is unlikely because a *G. ruber* $\delta^{18}O$ record from core M5-422 in the northwestern Arabian Sea shows opposing trends over the same time period (Cullen et al., 2000), and a local alkenone SST proxy record shows relatively higher temperatures in the same period (Doose-Rolinski et al., 2001). If the ~0.2‰ (relative to mean) increase in $\delta^{18}O$ of *G. ruber* at 4.1 ka BP was caused by temperature change rather than salinity, a ~1° C cooling of surface water would be required (Kim and O'Neil, 1997).

Following Staubwasser et al. (2003), we interpret the $\delta^{18}O$ variations of *G. ruber* to be predominantly a salinity signal. Salinity at the core site is dependent on changes in Indus River discharge, local run-off, and direct precipitation. Although the ISM would be the main influence on direct precipitation and run-off at the coring location, changes in the IWM could also influence Indus River discharge.

The thermocline-dwelling foraminifera *N. dutertrei* shows maximum abundances during winter, and are interpreted to reflect winter mixing. During weak IWM conditions, colder unmixed water would result in higher $\delta^{18}O$ values of *N. dutertrei*, whereas enhanced mixing and homogenization of the water column under strong IWM conditions would decrease $\delta^{18}O$. The minimum of $\delta^{18}O$ in *N. dutertrei* occurs between 4.5 and 4.3 ka BP, pointing to a period of strengthened IWM. We interpret the stepped increase in $\delta^{18}O$ of *N. dutertrei* at 4.1 ka BP to represent a decrease in IWM wind-driven mixing. Similarly, $\delta^{13}C$ of *N. dutertrei* increases significantly after 4.1 ka BP (Figure 3), which could indicate reduced upwelling of low $\delta^{13}C$ intermediate water (Lynch-Stieglitz, 2006; Ravelo and Hillaire-Marcel, 2007; Sautter and Thunell, 1991); however, the interpretation of $\delta^{13}C$ remains uncertain because of a poor understanding of the controls on the $\delta^{13}C$ of planktonic foraminifera in this region. According to the $\delta^{18}O$ signal of *N. dutertrei*, the temperature pattern in the thermocline implies surface cooling between 4.5 and 4.3 ka BP and surface warming after 4.1 ka BP interrupted only by a period of cooling between 3.7 and 3.3 ka BP, which is in broad agreement with records of alkenone sea-surface temperature estimates from cores in the northeastern Arabian Sea ("E" in Figure 1) (Doose-Rolinski et al., 2001; Staubwasser, 2012).

5.2 Interpretation of foraminifer $\Delta\delta^{18}O$

By using $\Delta\delta^{18}O$ between foraminifer species, we can distinguish additional processes affecting the surface waters and thermocline (Ravelo and Shackleton, 1995). This technique has been used previously to infer changes in the strength of the East Asian Winter Monsoon (EAWM) in the South China Sea (Tian et al., 2005), as well as mixed layer and thermocline depth in other studies (Billups et al., 1999; Cannariato and Ravelo, 1997; Norris, 1998). Here we use the difference in the $\delta^{18}O$ of *G. ruber* and *N. dutertrei* ($\Delta\delta^{18}O_{d-r}$) to track changes in the surface-to-deep gradient. This gradient can be driven by either $\delta^{18}O$ changes in the surface-dwelling (*G. ruber*) and/or the thermocline-dwelling species (*N. dutertrei*). During times of a strengthened winter monsoon, $\Delta\delta^{18}O_{d-r}$ will decrease as surface waters are homogenized and the thermocline deepens. Similarly, $\Delta\delta^{18}O_{d-r}$ will also decrease during times of a weakened summer monsoon, as decreased Indus River discharge will increase surface water salinity and $\delta^{18}O$ of *G. ruber* will become more similar to *N. dutertrei*.

G. sacculifer is also a surface dweller, but has a slightly deeper depth habitat than *G. ruber*. We thus expect *G. ruber* to be more influenced by surface salinity variations than *G. sacculifer*, and suggest the $\delta^{18}O$ difference between the two species ($\Delta\delta^{18}O_{s-r}$) reflects the influence of Indus River discharge on near surface salinity. The smallest difference in $\Delta\delta^{18}O_{s-r}$ occurs at 4.1 ka BP, which is interpreted as an increase in surface water salinity (Figure 6).

The difference in $\delta^{18}O$ between *G. sacculifer* and *N. dutertrei* ($\Delta\delta^{18}O_{d-s}$) also reflects surface mixing and thermocline depth, but *G. sacculifer* is less affected by surface salinity changes than *G. ruber*. Thus, the responses of $\Delta\delta^{18}O_{s-r}$ and $\Delta\delta^{18}O_{d-s}$ can be used to differentiate between surface water salinity changes and wind-driven mixing. Accordingly, simultaneously low $\Delta\delta^{18}O_{d-s}$ and $\Delta\delta^{18}O_{d-r}$ indicate a period of increased surface water mixing and increased IWM (such as the period between 4.5 and 4.3 ka BP), but times of relatively low $\Delta\delta^{18}O_{d-s}$ but high $\Delta\delta^{18}O_{d-r}$ and $\Delta\delta^{18}O_{s-r}$ (around 5.0 ka BP) indicate periods of increased Indus discharge and strength of the ISM and IWM.

The following period of low $\Delta\delta^{18}O_{d-r}$ from 4.1-3.9 ka BP is likely driven by increased salinity of surface water. This distinction becomes clearer when examining the $\Delta\delta^{18}O_{s-r}$, where increased similarity from 4.8-3.9 ka BP (with a sharp increase at 4.1 ka BP) reflects the effect of increased sea surface salinity that reduces the $\delta^{18}O$ difference between *G. ruber* and *G. sacculifer*. At the same time, weakened winter mixing increases $\Delta\delta^{18}O_{d-s}$, which occurs from 4.2-3.9 ka BP. Importantly, the proxies also indicate that increased IWM mixing is generally positively correlated with increased Indus discharge, and vice versa. The single time period when this does not hold true is 4.5-4.25 ka BP, when increased IWM mixing is coupled with decreased Indus discharge.

In summary, our multi-species approach using $\delta^{18}O$ of *G. ruber*, *G. sacculifer*, and *N. dutertrei* allows us to differentiate between strength of the IWM and freshwater discharge of the Indus River. We suggest that ISM strength decreased gradually from at least 4.8 ka BP, while the IWM strength peaked around 4.5-4.3 ka BP and then weakened afterwards. It is unlikely that the abrupt increase in *G. ruber* $\delta^{18}O$ at 4.1 ka BP and low $\Delta\delta^{18}O_{s-r}$ could be caused solely by the decrease in IWM strength, even though IWM contributes to Indus River discharge. Weakening of the ISM must have played a substantial role in the 4.1 ka BP shift as well, indicated by the period 4.5-4.25 ka BP, when Indus discharge reflected a weak ISM ($\Delta\delta^{18}O_{s-r}$) despite a phase of strengthened IWM.

5.3 Comparison to marine records

Other marine records from the Arabian Sea also suggest a gradual decrease in ISM strength from ~5 ka BP (Gupta et al., 2003; Overpeck et al., 1996). Cullen et al. (2000) observed an abrupt peak in aeolian dolomite and calcite in marine sediments in the Gulf of Oman from 4.0-3.6 ka BP, and Ponton et al. (2012) also showed a shift to weaker ISM after 4.0 ka BP in the Bay of Bengal, based on $\delta^{13}C$ of leaf waxes. Marine IWM reconstructions are not particularly coherent: although Doose-Rolinski et al. (2001) find a decrease in evaporation and weakening of the ISM between 4.6 and 3.7 ka BP, they argue this was accompanied by a relative increase in IWM strength. Giosan et al. (2018) inferred enhanced winter monsoon conditions from 4.5-3.0 ka BP based on a planktic paleo-DNA and % *Globigerina falconensis* record close to our coring site ("C" in Figure 1), which disagrees with our finding of decreased upper ocean mixing after 4.3 ka BP. We suggest that the high stratigraphic (i.e., laminated) and chronological (i.e., 15 radiocarbon dates between 5.4-3.0 ka BP) resolution of core 63KA paired with a multi-species foraminifer $\delta^{18}O$ record provides a robust history of the timing of changes in IWM and ISM strength, but additional studies are needed to resolve some of the discrepancies among the records.

5.4 Comparison to regional terrestrial records

The 63KA $\delta^{18}O$ record obtained from three foraminifer species highlights several important ocean-atmosphere changes over the 5.4-3.0 ka BP time period. First, a sharp decrease occurred in both summer and winter precipitation at 4.1 ka BP, which is within a broader 300-year period of increased aridity spanning both rainfall seasons between 4.2 and 3.9 ka BP. In detail, we infer a relative decrease in Indus River discharge and weakened ISM between 4.8 and 3.9 ka BP, peaking at 4.1 ka BP, while a 200-year-long interval of strong IWM interrupted this period from 4.5-4.3 ka BP. Furthermore, the stepped change in $\delta^{18}O$ of *N. dutertrei* suggests an enduring change in ocean-atmosphere conditions after 4.1 ka BP.

A relatively abrupt ~4.2 ka BP climate event has been observed in several terrestrial records on the Indian subcontinent, most notably Mawmluh Cave (~4.1-3.9 ka BP) in northeastern India (Berkelhammer et al., 2012) and Kotla Dahar (~4.1 ka BP) in northwestern India (Dixit et al., 2014) (Figure 7). A less abrupt yet still arid period is documented in a peat profile (~4.0-3.5 ka BP) from northcentral India (Phadtare, 2000), at Lonar Lake (~4.6-3.9 ka BP) in central India (Menzel et al., 2014), and at Rara Lake (~4.2-3.7 ka BP) in western Nepal (Nakamura et al., 2016). Finally, a recent study of oxygen and hydrogen isotopes in gypsum hydration water from Karsandi on the northern margin of the Thar Desert showed wet conditions between 5.1 and 4.4 ka BP, after which the playa lake dried out sometime between 4.4 and 3.2 ka BP (Dixit et al., 2018). Considering terrestrial records can record more local climatic conditions than marine records, it is remarkable that the records collectively agree on a period of regional aridity between 4.2 and 3.9 ka BP within the uncertainties of the age models that vary considerably among records.

However, not all records support this finding. For example, a reconstruction from Sahiya Cave in northwestern India shows an abrupt decrease in $\delta^{18}O$ interpreted to reflect an increase in monsoon strength from ~4.3-4.15 ka BP, followed by an arid trend after 4.15 ka BP (Kathayat et al., 2017). In addition, several other Thar Desert records do not identify a "4.2 ka BP event" *sensu stricto*, but instead suggest that lakes dried out several centuries earlier (Deotare et al., 2004; Enzel et al., 1999; Singh et al., 1990) or later (Sinha et al., 2006) than 4.2 ka BP. This discrepancy may relate to non-linear climate responses of lakes, which would not record a drought at 4.2 ka BP if they had already dried out earlier from the ongoing decrease in summer rainfall. In addition, there are also significant concerns about chronological uncertainties from the use of radiocarbon of bulk sediment for dating in some of these records. It is also possible that variations in the timing of climate change inferred from the terrestrial records may be real, reflecting different sensitivity to ISM and IWM rain. As a marine record, core 63KA integrates large-scale ocean-atmosphere changes, and therefore can help inform the interpretation of the more locally sensitive terrestrial records.

More distantly, several terrestrial records in the Middle East also show a decrease in winter precipitation proxies around 4.2 ka BP: Jeita Cave in Lebanon records a relatively dry period between 4.4 and 3.9 ka BP (Cheng et al., 2015) and Soreq Cave in Israel shows a period of increased aridity starting at ~4.3 ka BP (Bar-Matthews et al., 2003; Bar-Matthews and Ayalon, 2011) (Figure 8). Lake Van in eastern Turkey also records reduced spring rainfall and enhanced aridity after ~4.0 ka BP (Wick et al., 2003; Lemcke and Sturm, 1997). All of these records suggest a relatively arid period with reduced winter precipitation after ~4.3 ka BP, as inferred from core 63KA. Qunf Cave in Oman (Fleitmann et al., 2003), which is outside the range of IWM influence, instead shows a steady mid-Holocene weakening of the ISM that closely follows trends in summer solar insolation.

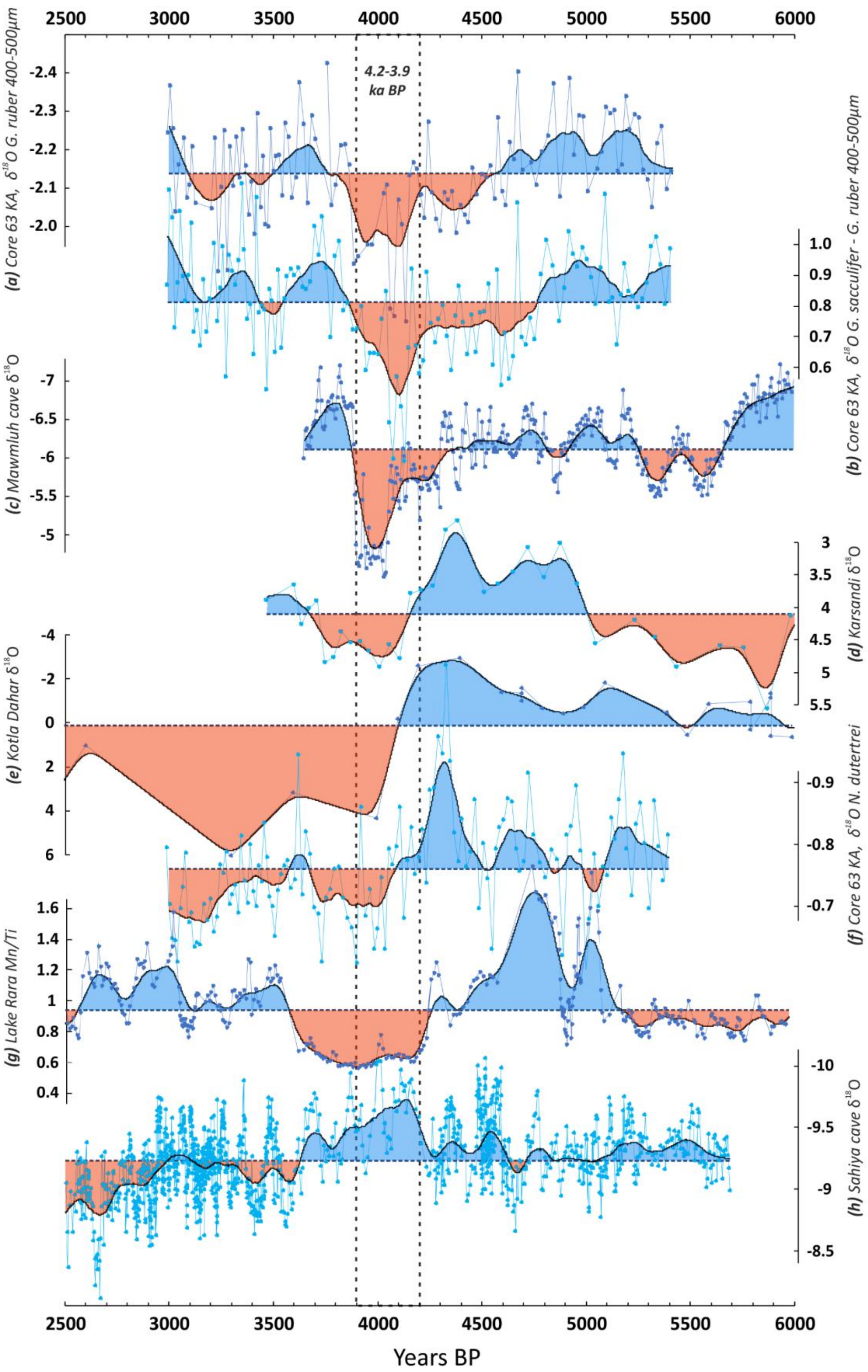

Figure 7. Comparison of the $\delta^{18}O$ record of core 63KA with terrestrial records from the Indian Subcontinent, from top to bottom: **a.** and **b.** this study; **c.** Berkelhammer et al., 2012; **d.** Dixit et al., 2018; **e.** Dixit et al., 2014; **f.** this study; **g.** Nakamura et al., 2016; **h.** Kathayat et al., 2017. The mean

value for each record indicated by the horizontal dashed lines is taken for all available data between 6.0-2.5 ka BP.

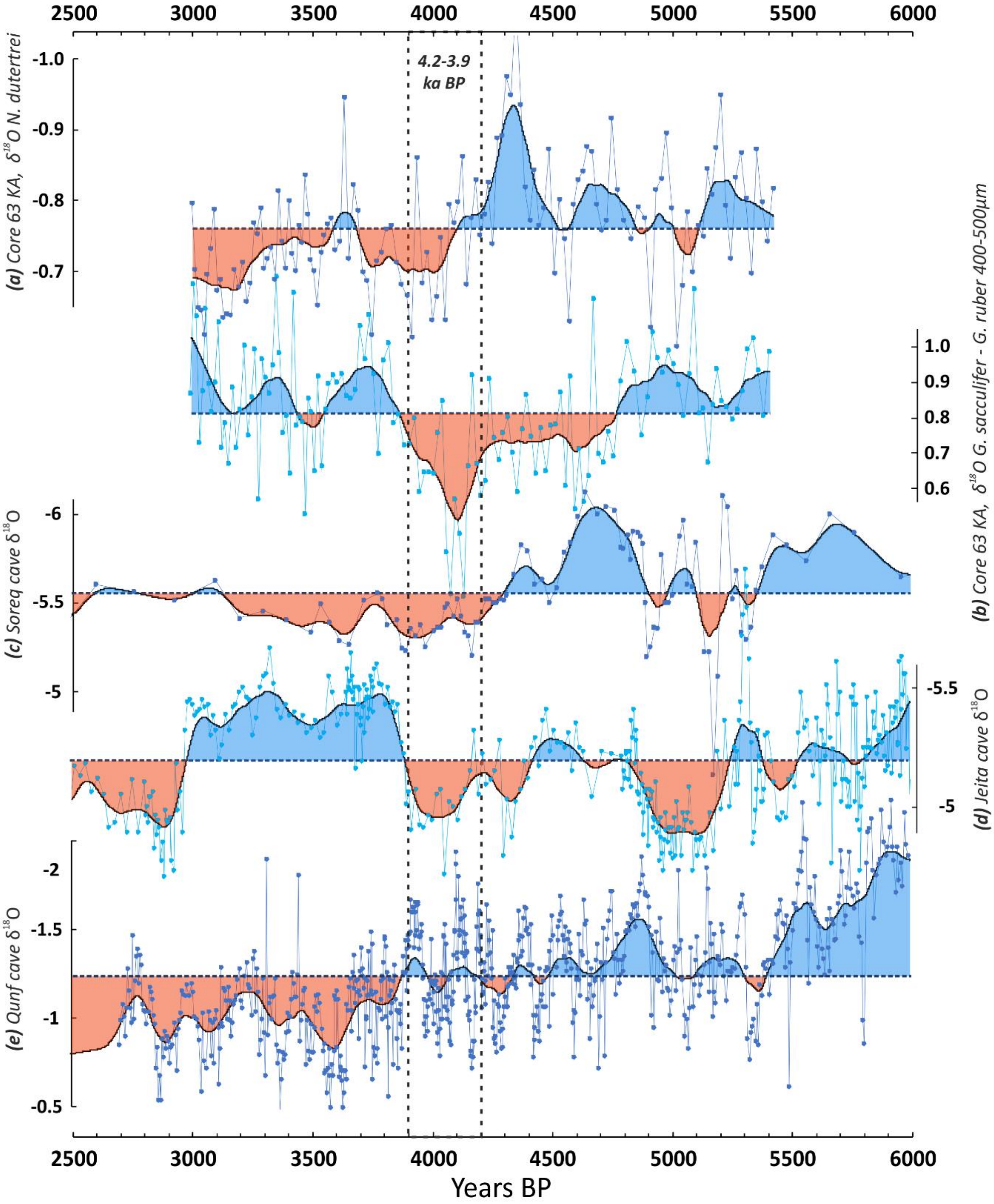

Figure 8. Comparison of the δ^{18}O record of core 63KA with more distant records: **a.** and **b.** this study; **c.** Bar-Matthews et al., 2003; **d.** Cheng et al., 2015; **e.** Fleitmann et al., 2003. The mean value for each record indicated by the horizontal dashed lines is taken for all available data between 6.0-2.5 ka BP.

5.5 Cultural impacts

On the basis of our reconstruction of reduced IWM mixing after 4.3 ka BP, accompanied by decreased freshwater discharge of the Indus River, it is worth considering what impacts could be expected from a reduction in IWM and ISM precipitation. A weakened IWM overlying a reduced or more variable ISM would likely result in a distinct climate signal over the Indus River catchment, with broad implications for seasonal river flow and water availability throughout the year. The presence of the two rainfall systems creates a complex and diverse range of environments and ecologies across northwest South Asia (Petrie et al., 2017). In a situation when rainfall in both seasons is reduced over extended periods, step-shifts in the natural environment may occur that are difficult to reverse (e.g., desertification, lake desiccation, regional vegetation changes, decline in overbank flooding and shift in river avulsion patterns).

Societies reliant on IWM, ISM, or a combination of the two would have been vulnerable to years with monsoon failure, and a shift affecting both seasons will have challenged resilience and tested sustainability (Green and Bates et al. in press; Petrie et al., 2017). Archaeological research into the transition from the urban Mature Harappan phase (~4.6-3.9 ka BP) to the post-urban Late Harappan phase (~3.9-3.6 ka BP) notes progressive deurbanization through the abandonment of large Indus cities and a depopulation of the most western Indus regions, concurrent with a general trend towards an increase of concentrations of rural settlements in some areas of the eastern Indus extent (Green and Petrie, 2018; Petrie et al., 2017; Possehl, 1997) (Figure S6). The relatively limited range of well-resolved available archaeobotanical data suggests that there was a degree of diversity in crop choice and farming strategies in different parts of the Indus Civilization across this time span (Petrie et al., 2016; Petrie and Bates, 2017; Weber, 1999; Weber et al., 2010). Farmers in southerly regions appear to have focused on summer or winter crops, while the more northern regions of Pakistan Punjab and Indian Punjab and Haryana were capable of supporting combinations of winter and summer crops (Petrie and Bates, 2017). Although there is evidence for diverse cropping practices involving both summer and winter crops in the northern areas during the urban period, agricultural strategies appeared to favor more intensive use of drought-resistant summer crops in the Late Harappan period (Madella and Fuller, 2006; Petrie and Bates, 2017; Pokharia et al., 2017; Weber, 2003; Wright, 2010). It has previously been suggested that weakened ISM was a major factor in these shifts (e.g. Giosan et al., 2012; Madella and Fuller, 2006). Based on our reconstruction of decreased IWM in northwest South Asia after 4.3 ka BP with a step-shift at 4.1 ka BP, we suggest that both IWM and ISM climatic factors played a role in shaping the human landscape. This includes the redistribution of population to smaller settlements in eastern regions with more direct summer rain, as well as the shift to increased summer crop dominated cropping strategies.

6. Conclusion

This study expanded on the $\delta^{18}O$ record of planktonic foraminifer in core 63KA of the northeastern Arabian Sea, originally published by Staubwasser et al. (2003). Using $\delta^{18}O$ of the surface-dwelling foraminifera *G. ruber*, the original study inferred an abrupt reduction in Indus River discharge at ~4.2 ka BP. Our further $\delta^{18}O$ analysis of a larger size fraction of this species corroborates maximum salinity at 4.1 and 3.95 ka BP. In addition, the $\delta^{18}O$ difference between the surface-dwelling *G. ruber* and slightly deeper-dwelling *G. sacculifer* ($\Delta\delta^{18}O_{s-r}$) reveals that surface waters were more saline than average for the period from 4.8-3.9 ka BP.

By also measuring a thermocline-dwelling planktonic foraminiferal species, *N. dutertrei*, we infer an increase in the strength of the IWM between 4.5 and 4.3 ka BP, followed by reduction in IWM-driven mixing that reaches a minimum at 4.1 ka BP.

Assuming that weaker IWM mixing implies a reduction in IWM rainfall amount or duration over northwest South Asia under past climatic conditions, the 63KA core is used to infer important changes in seasonal hydrology of the Indus River catchment. We propose that a combined weakening of the IWM and ISM at 4.1 ka BP led to what has been termed the "4.2 ka BP" drought over northwest South Asia. The intersection of both a gradually weakening ISM since 4.8 ka BP and a maximum decrease in IWM strength at 4.1 ka BP resulted in a spatially layered and heterogeneous drought over a seasonal to annual timescale. Regions in the western part of the Indus River basin accustomed to relying mainly on winter rainfall (also via river run-off) would have been most severely affected by such changes. Regions in the northeastern and eastern extents benefitted more from summer rainfall, and would have been less severely affected, particularly as the ISM appears to recover strength by 3.9 ka BP.

Relatively strengthened IWM surface water mixing between 4.5 and 4.3 ka BP correlates with a period of higher precipitation recorded at Karsandi on the northern margin of the Thar Desert (Dixit et al., 2018), an area within the summer rainfall zone that is also sensitive to small changes in winter precipitation. This time span also represents the beginnings of the Mature Harappan phase (Possehl, 2002; Wright, 2010), which implies that increasingly urbanized settlements may have flourished under a strengthened IWM. With a weakening of the IWM at ~4.1 ka, eastern regions with more access to ISM rainfall may have been more favorable locations for agriculture. This may also help explain the broad shift in population towards more rural settlements in the northeastern extent of the Indus Civilization that occurred by ~3.9 ka BP (Possehl, 1997; Petrie et al., 2017), and a shift to more drought-tolerant kharif (summer) season crops in Gujarat (Pokharia et al., 2017) and at Harappa (Madella and Fuller, 2006; Weber, 2003).

Given the importance of the relationships between humans and the environment during the time of the Indus Civilization, understanding the impact of the IWM on precipitation variability in northwest South Asia remains a critical area of research. We especially need a better understanding of the wind patterns and moisture pathways that controlled the IWM in the past. Disentangling both the length and intensity of seasonal precipitation is a crucial aspect of understanding the impact of climate change on past societies, particularly in a diverse region relying on mixed water sources (e.g., fluvial, ground aquifer, direct rainfall).

Data availability

Data presented in the paper can be accessed by contacting the corresponding author or online at http://eprints.esc.cam.ac.uk/id/eprint/4371.

Author contributions

M.S. supplied core 63KA material, A.G. prepared the material for isotopic measurements, and A.G. and D.A.H. interpreted the results. A.G., D.A.H., and C.A.P. wrote the manuscript.

Competing interests

The authors declare that they have no conflict of interest.

Acknowledgements

This research was carried out as part of the *TwoRains* project, which is supported by funding from the European Research Council (ERC) under the European Union's Horizon 2020 research and innovation programme (grant agreement no 648609). The authors thank the following persons at the University of Cambridge: Maryline Vautravers for foraminifera identification, James Rolfe and John Nicolson for $\delta^{18}O$ measurements. We also thank our editor and reviewers for comments that improved the manuscript.

References

Agrawal, D. P.: The Indus Civilization: an interdisciplinary perspective, Aryan Books International, New Delhi, India, 2007.

Ahmad, N., Mohammad, A., and Khan, S. T.: Country Report on Water resources of Pakistan, in South Asia Water Balance Workshop. Hansen Institute for World Peace, San Diego, California, USA, 30 April – 2 May 2001, 2001.

Banse, K.: Overview of the hydrography and associated biological phenomena in the Arabian Sea off Pakistan, in Marine Geology and Oceanography of the Arabian Sea and Coastal Pakistan, Ed. Haq, B. U., and Milliman, J. D., pp. 273-301, Van Nostrand Reinhold, New York, 1984.

Bar-Matthews, M., and Ayalon, A.: Mid-Holocene climate variations revealed by high-resolution speleothem records from Soreq Cave, Israel and their correlation with cultural changes, The Holocene, 21, 163-171, 2011.

Bar-Matthews, M., Ayalon, A., Gilmour, M., Matthews, A., and Hawkesworth, C. J.: Sea–land oxygen isotopic relationships from planktonic foraminifera and speleothems in the Eastern Mediterranean region and their implication for paleorainfall during interglacial intervals, Geochimica et Cosmochimica Acta, 67, 3181-3199, 2003.

Bé, A. W., and Hutson, W. H.: Ecology of planktonic foraminifera and biogeographic patterns of life and fossil assemblages in the Indian Ocean, Micropaleontology, 369-414, 1977.

Bemis, B. E., Spero, H. J., Bijma, J., and Lea, D. W.: Reevaluation of the oxygen isotopic composition of planktonic foraminifera: Experimental results and revised paleotemperature equations. Paleoceanography, 13, 150-160, 1998.

Berkelhammer, M., Sinha, A., Stott, L., Cheng, H., Pausata, F. S., and Yoshimura, K.: An abrupt shift in the Indian monsoon 4000 years ago, Geophys. Monogr. Ser, 198, 2012.

Billups, K., Ravelo, A. C., Zachos, J. C., and Norris, R. D.: Link between oceanic heat transport, thermohaline circulation, and the Intertropical Convergence Zone in the early Pliocene Atlantic, Geology, 27, 319-322, 1999.

Blaauw, M., and Christen, J. A.: Flexible paleoclimate age-depth models using an autoregressive gamma process, Bayesian analysis, 6, 457-474, 2011.

Chaudhuri, P., and Marron, J. S.: SiZer for exploration of structures in curves, Journal of the American Statistical Association, 94, 807-823, 1999.

Cheng, H., Sinha, A., Verheyden, S., Nader, F. H., Li, X. L., Zhang, P. Z., Yin, J. J., Yi, L., Peng., Y. B., Rao, Z. G., Ning, Y. F., and Edwards, R. L.: The climate variability in northern Levant over the past 20,000 years, Geophysical Research Letters, 42, 8641-8650, 2015.

Cannariato, K.G., and Ravelo, A.C.: Pliocene-Pleistocene evolution of eastern tropical Pacific surface water circulation and thermocline depth. Paleoceanography, 12, 805-820, doi: 10.1029/97PA02514, 1997.

Cayre, O., and Bassinot, F.: Oxygen isotope composition of planktonic foraminiferal shells over the Indian Ocean: calibration to modern oceanographic data. Mineral Mag, 62, 288-289, 1998.

Curry, W. B., Ostermann, D. R., Guptha, M. V. S., and Ittekkot, V.: Foraminiferal production and monsoonal upwelling in the Arabian Sea: evidence from sediment traps, Geological Society, London, Special Publications, 64, 93-106, 1992.

Cullen, H. M., deMenocal, P. B., Hemming, S., Hemming, G., Brown, F. H., Guilderson, T., and Sirocko, F.: Climate change and the collapse of the Akkadian empire: Evidence from the deep sea, Geology, 28, 379-382, 2000.

Dahl, K. A., and Oppo, D. W.: Sea surface temperature pattern reconstructions in the Arabian Sea, Paleoceanography, 21, 2006.

Deotare, B. C., Kajale, M. D., Rajaguru, S. N., Kusumgar, S., Jull, A. J. T., and Donahue, J. D.: Palaeoenvironmental history of Bap-Malar and Kanod playas of western Rajasthan, Thar desert, Journal of Earth System Science, 113, 403-425, 2004.

Dimri, A. P.: Surface and upper air fields during extreme winter precipitation over the western Himalayas, Pure and Applied Geophysics, 163, 1679-1698, 2006.

Dimri, A. P., and Dash, S. K.: Wintertime climatic trends in the western Himalayas. Climatic Change, 111, 775-800, 2012.

Dixit, Y., Hodell, D. A., and Petrie, C. A.: Abrupt weakening of the summer monsoon in northwest India ~4100 yr ago, Geology, 42, 339-342, 2014.

Dixit, Y., Hodell, D. A., Giesche, A., Tandon, S. K., Gázquez, F., Saini, H. S., Skinner, L. C., Mujtaba, S. A. I., Pawar, V., Singh, R.N., and Petrie, C. A.: Intensified summer monsoon and the urbanization of Indus Civilization in northwest India, Scientific reports, 8, 4225, 2018.

Doose-Rolinski, H., Rogalla, U., Scheeder, G., Lückge, A., and Rad, U.: High-resolution temperature and evaporation changes during the late Holocene in the northeastern Arabian Sea, Paleoceanography and Paleoclimatology, 16, 358-367, 2001.

Duplessy, J. C., Labeyrie, L., Arnold, M., Paterne, M., Duprat, J., and van Weering, T. C.: Changes in surface salinity of the North Atlantic Ocean during the last deglaciation. Nature, 358, 485, 1992.

Enzel, Y., Ely, L. L., Mishra, S., Ramesh, R., Amit, R., Lazar, B., Rajaguru, S.N., Baker, V. R., and Sandler, A.: High-resolution Holocene environmental changes in the Thar Desert, northwestern India, Science, 284, 125-128, 1999.

Farmer, E. C., Kaplan, A., de Menocal, P. B., and Lynch-Stieglitz, J.: Corroborating ecological depth preferences of planktonic foraminifera in the tropical Atlantic with the stable oxygen isotope ratios of core top specimens, Paleoceanography, 22, 2007.

Finné, M., Holmgren, K., Sundqvist, H. S., Weiberg, E., and Lindblom, M.: Climate in the eastern Mediterranean, and adjacent regions, during the past 6000 years–A review, Journal of Archaeological Science, 38, 3153-3173, 2011.

Fleitmann, D., Burns, S. J., Mudelsee, M., Neff, U., Kramers, J., Mangini, A., and Matter, A.: Holocene forcing of the Indian monsoon recorded in a stalagmite from southern Oman, Science, 300, 1737-1739, 2003.
Gadgil, S.: The Indian monsoon and its variability, Annual Review of Earth and Planetary Sciences, 31, 429-467, 2003.
Giosan, L., Clift, P. D., Macklin, M. G., Fuller, D. Q., Constantinescu, S., Durcan, J. A., Stevens, T., Duller, G. A. T., Tabrez, A. R., Gangal, K., Adhikari, R., Alizai, A., Filip, F., VanLaningham, S., and Syvitski, J. P. M.: Fluvial landscapes of the Harappan civilization, Proceedings of the National Academy of Sciences, 109, E1688-E1694, 2012.
Giosan, L., Orsi, W. D., Coolen, M., Wuchter, C., Dunlea, A. G., Thirumalai, K., Munoz, S. E., Clift, P. D., Donnelly, J. P., Galy, V., and Fuller, D. Q.: Neoglacial Climate Anomalies and the Harappan Metamorphosis, Climate of the Past, 14, 1669-1686, , 2018.
Green, A. S., Bates, J., Acabado, S., Coutros, P., Glover, J., Miller, N., Sharratt, N., and Petrie, C.A.: How to Last a Millennium; Or a Global Perspective on the Long-Term Dynamics of Human Sustainability, in press (under review) for Nature Sustainability.
Green, A. S., and Petrie, C. A.: Landscapes of Urbanization and De-Urbanization: A Large-Scale Approach to Investigating the Indus Civilization's Settlement Distributions in Northwest India, Journal of Field Archaeology, 1-16, 2018.
Gupta, A. K., Anderson, D. M., and Overpeck, J. T.: Abrupt changes in the Asian southwest monsoon during the Holocene and their links to the North Atlantic Ocean. Nature, 421, 354, 2003.
Hastenrath, S., and Lamb, P. J.: Climatic atlas of the Indian Ocean. Part II: The oceanic heat budget, Wisconsin University Press, Madison, Wisconsin, USA, 93, 17, 1979.
Hatwar, H. R., Yadav, B. P., and Rao, Y. R.: Prediction of western disturbances and associated weather over Western Himalayas, Current science, 913-920, 2005.
Hemleben, C., Spindler, M., and Anderson, O. R.: Modern planktonic foraminifera. Springer Science and Business Media, 2012.
Joseph, S., and Freeland, H. J.: Salinity variability in the Arabian Sea. Geophysical research letters, 32, 2005.
Karim, A., and Veizer, J.: Water balance of the Indus River Basin and moisture source in the Karakoram and western Himalayas: Implications from hydrogen and oxygen isotopes in river water, Journal of Geophysical Research: Atmospheres, 107, ACH-9, 2002.
Kathayat, G., Cheng, H., Sinha, A., Yi, L., Li, X., Zhang, H., Li, H., Ning, Y., and Edwards, R. L.: The Indian monsoon variability and civilization changes in the Indian subcontinent, Science advances, 3, e1701296, 2017.
Kim, S. T., and O'Neil, J. R.: Equilibrium and nonequilibrium oxygen isotope effects in synthetic carbonates, Geochimica et Cosmochimica Acta, 61, 3461-3475, 1997.
Kumar, S. P., and Prasad, T. G.: Formation and spreading of Arabian Sea high-salinity water mass, Journal of Geophysical Research: Oceans, 104, 1455-1464, 1999.
Lemcke, G., and Sturm, M.: $\delta^{18}O$ and trace element measurements as proxy for the reconstruction of climate changes at Lake Van (Turkey): Preliminary results, in Third millennium BC climate change and Old World collapse, Springer, Berlin, Heidelberg, Germany, 653-678, 1997.
Locarnini, R. A., Mishonov, A. V., Antonov, J. I., Boyer, T. P., Garcia, H. E., Baranova, O. K., Zweng, M. M., Paver, C. R., Reagan, J. R., Johnson, D. R., Hamilton, M., and Seidov, D.: World Ocean Atlas 2013, Volume 1: Temperature. S. Levitus, Ed., A. Mishonov Technical Ed., NOAA Atlas NESDIS 73, 40 pp., 2013.

Lynch-Stieglitz, J.: Tracers of past ocean circulation, in: Treatise on geochemistry, 6, Elderfield, H., Holland, H. D., and Turekian, K. K. (Eds), Elsevier, 433-451, 2006.

Madella, M., and Fuller, D. Q.: Palaeoecology and the Harappan Civilisation of South Asia: a reconsideration, Quaternary Science Reviews, 25, 1283-1301, 2006.

Madhupratap, M., Kumar, S. P., Bhattathiri, P. M. A., Kumar, M. D., Raghukumar, S., Nair, K. K. C., and Ramaiah, N.: Mechanism of the biological response to winter cooling in the northeastern Arabian Sea, Nature, 384, 549-552, 1996.

Maslin, M. A., Shackleton, N. J., and Pflaumann, U.: Surface water temperature, salinity, and density changes in the northeast Atlantic during the last 45,000 years: Heinrich events, deep water formation, and climatic rebounds, Paleoceanography, 10, 527-544, 1995.

Mayewski, P. A., Rohling, E. E., Stager, J. C., Karlén, W., Maasch, K. A., Meeker, L. D., Meyerson, E. A., Gasse, F., van Kreveld, S., Holmgren, K., Lee-Thorp, J., Rosqvist, G., Rack, F., Staubwasser, M., Schneider, R.R., and Steig, E.J.: Holocene climate variability, Quaternary research, 62, 243-255, 2004.

Menzel, P., Gaye, B., Mishra, P. K., Anoop, A., Basavaiah, N., Marwan, N., Plessen, B., Prasad, S., Riedel, N., Stebich, M., and Wiesner, M. G.: Linking Holocene drying trends from Lonar Lake in monsoonal central India to North Atlantic cooling events, Palaeogeography, palaeoclimatology, palaeoecology, 410, 164-178, 2014.

Nakamura, A., Yokoyama, Y., Maemoku, H., Yagi, H., Okamura, M., Matsuoka, H., Miyake, N., Osada, T., Adhikari, D. P., Dangol, V., Ikehara, M., Miyairi, Y., and Matsuzaki, H.: Weak monsoon event at 4.2 ka recorded in sediment from Lake Rara, Himalayas, Quaternary International, 397, 349-359, 2016.

Norris, R. D.: Planktonic foraminifer biostratigraphy: eastern equatorial Atlantic, in: Proceedings of the Ocean Drilling Program: Scientific results, 159, 445-479, 1998.

Overpeck, J., Anderson, D., Trumbore, S., and Prell, W.: The southwest Indian Monsoon over the last 18000 years. Climate Dynamics, 12, 213-225, 1996.

Petrie, C. A., and Bates, J.: 'Multi-cropping', Intercropping and Adaptation to Variable Environments in Indus South Asia. Journal of World Prehistory, 30, 81-130, 2017.

Petrie, C. A., Bates, J., Higham, T., and Singh, R. N.: Feeding ancient cities in South Asia: dating the adoption of rice, millet and tropical pulses in the Indus civilisation. Antiquity, 90, 1489-1504, 2016.

Petrie, C. A., Singh, R. N., Bates, J., Dixit, Y., French, C. A., Hodell, D. A., Pandey, A. K., Parikh, D., Pawar, V., Redhouse, D. I., and Singh, D. P.: Adaptation to variable environments, resilience to climate change: Investigating land, water and settlement in Indus Northwest India, Current Anthropology, 58, 2017.

Phadtare, N. R.: Sharp decrease in summer monsoon strength 4000–3500 cal yr BP in the Central Higher Himalaya of India based on pollen evidence from alpine peat, Quaternary Research, 53, 122-129, 2000.

Pokharia, A. K., Agnihotri, R., Sharma, S., Bajpai, S., Nath, J., Kumaran, R. N., and Negi, B. C.: Altered cropping pattern and cultural continuation with declined prosperity following abrupt and extreme arid event at ~4,200 yrs BP: Evidence from an Indus archaeological site Khirsara, Gujarat, western India, PloS one, 12, 2017.

Ponton, C., Giosan, L., Eglinton, T. I., Fuller, D. Q., Johnson, J. E., Kumar, P., and Collett, T. S.: Holocene aridification of India, Geophysical Research Letters, 39, 2012.

Possehl, G. L.: The transformation of the Indus civilization, Journal of World Prehistory, 11, 425-472, 1997.

Possehl, G. L.: The Indus Civilization: a Contemporary Perspective. Rowman Altamira, 2002.

Possehl, G. L.: The Indus Civilization: an introduction to environment, subsistence, and cultural history. Indus ethnobiology, 1-20, 2003.
Prasad, S., and Enzel, Y.: Holocene paleoclimates of India. Quaternary Research, 66, 442-453, 2006.
Ramasastri, K.S.: Snow melt modeling studies in India, in: The Himalayan Environment, S.K. Dash and J. Bahadur (Eds.), New Age International, 59–70, 1999.
Rangachary, N., and Bandyopadhyay, B. K.: An analysis of the synoptic weather pattern associated with extensive avalanching in Western Himalaya, Int. Assoc. of Hydrol. Sci. Publ, 162, 311-316, 1987.
Ravelo, A. C., and Hillaire-Marcel, C.: Chapter Eighteen the use of oxygen and carbon isotopes of foraminifera in Paleoceanography, Developments in Marine Geology, 1, 735-764, 2007.
Ravelo, A.C., and Shackleton, N.J.: Evidence for surface-water circulation changes at Site 851 in the eastern Tropical Pacific Ocean, in: Proceedings of the Ocean Drilling Program, Scientific Results, College Station, TX (Ocean Drilling Program), Pisias, N. G.; Mayer, L. A.; Janecek, T. R.; Palmer-Julson, A.; van Andel, T. H. (Eds.), 138, 503-514, doi: 10.2973/odp.proc.sr.138.126, 1995.
Reimer, P. J., Bard, E., Bayliss, A., Beck, J. W., Blackwell, P. G., Ramsey, C. B., Buck, C. E., Cheng, H., Edwards, R. L., Friedrich, M., Grootes, P. M., Guilderson, T. P., Haflidason, H., Hajdas, I., Hatté, C., Heaton, T. J., Hoffmann, D. L., Hogg, A. G., Hughen, K. A., Kaiser, K. F., Kromer, B., Manning, St.W., Niu, M., Reimer, R. W., Richards, D. A., Scott, E. M., Southon, J. R., Staff, R. A., Turney, C. S. M., and van der Plicht, J.: IntCal13 and Marine13 radiocarbon age calibration curves 0–50,000 years cal BP, Radiocarbon, 55, 1869-1887, 2013.
Rohling, E. J.: Paleosalinity: confidence limits and future applications, Marine Geology, 163, 1-11, 2000.
Sautter, L. R., and Thunell, R. C.: Seasonal variability in the $\delta^{18}O$ and $\delta^{13}C$ of planktonic foraminifera from an upwelling environment: sediment trap results from the San Pedro Basin, Southern California Bight. Paleoceanography, 6, 307-334, 1991.
Schneider, U., Becker, A., Finger, P., Meyer-Christoffer, A., Bruno, R., and Ziese, M.: GPCC Full Data Reanalysis Version 7.0 at 0.5°: Monthly Land-Surface Precipitation from Rain-Gauges built on GTS-based and Historic Data, Deutscher Wetterdienst/Global Precipitation Climatology Centre, 2015.
Schulz, H., von Rad, U., and Ittekkot, V.: Planktic foraminifera, particle flux and oceanic productivity off Pakistan, NE Arabian Sea: modern analogues and application to the palaeoclimatic record, Geological Society, London, Special Publications, 195, 499-516, 2002.
Shackleton, N. J.: Attainment of isotopic equilibrium between ocean water and the benthonic foraminifera genus Uvigerina: isotopic changes in the ocean during the last glacial, Colloques Internationaux du C.N.R.S., 1974.
Shenoi, S. S. C., Shankar, D., and Shetye, S. R.: Differences in heat budgets of the near-surface Arabian Sea and Bay of Bengal: Implications for the summer monsoon, Journal of Geophysical Research: Oceans, 107, 5-1, 2002.
Singh, G., Wasson, R. J., and Agrawal, D. P.: Vegetational and seasonal climatic changes since the last full glacial in the Thar Desert, northwestern India, Review of Palaeobotany and Palynology, 64, 351-358, 1990.

Sinha, R., Smykatz-Kloss, W., Stüben, D., Harrison, S. P., Berner, Z., and Kramar, U.: Late Quaternary palaeoclimatic reconstruction from the lacustrine sediments of the Sambhar playa core, Thar Desert margin, India, Palaeogeography, Palaeoclimatology, Palaeoecology, 233, 252-270, 2006.

Sirocko, F.: Deep-sea sediments of the Arabian Sea: A paleoclimatic record of the southwest-Asian summer monsoon, Geologische Rundschau, 80, 557-566, 1991.

Sonderegger, D. L., Wang, H., Clements, W. H., and Noon, B. R.: Using SiZer to detect thresholds in ecological data, Frontiers in Ecology and the Environment, 7, 190-195, 2009.

Staubwasser, M., Sirocko, F., Grootes, P. M., and Erlenkeuser, H.: South Asian monsoon climate change and radiocarbon in the Arabian Sea during early and middle Holocene, Paleoceanography and Paleoclimatology, 17, 2002.

Staubwasser, M., Sirocko, F., Grootes, P. M., and Segl, M.: Climate change at the 4.2 ka BP termination of the Indus valley civilization and Holocene south Asian monsoon variability, Geophysical Research Letters, 30, 2003.

Staubwasser, M., and Weiss, H.: Holocene climate and cultural evolution in late prehistoric–early historic West Asia, Quaternary Research, 66, 372-387, 2006.

Staubwasser, M.: Late Holocene Drought Pattern Over West Asia. Climates, Landscapes, and Civilizations, 89-96, 2012.

Steinke, S., Mohtadi, M., Groeneveld, J., Lin, L. C., Löwemark, L., Chen, M. T., and Rendle-Bühring, R.: Reconstructing the southern South China Sea upper water column structure since the Last Glacial Maximum: Implications for the East Asian winter monsoon development, Paleoceanography and Paleoclimatology, 25, 2010.

Steph, S., Regenberg, M., Tiedemann, R., Mulitza, S., and Nürnberg, D.: Stable isotopes of planktonic foraminifera from tropical Atlantic/Caribbean core-tops: Implications for reconstructing upper ocean stratification. Marine Micropaleontology, 71, 1-19, 2009.

Tian, J., Wang, P., Chen, R., and Cheng, X.: Quaternary upper ocean thermal gradient variations in the South China Sea: Implications for east Asian monsoon climate, Paleoceanography, 20, 2005.

Von Rad, U., Schulz, H., Khan, A. A., Ansari, M., Berner, U., Čepek, P., Cowie, G., Dietrich, P., Erlenkeuser, H., Geyh, M., Jennerjahn, T., Lückge, A., Marchig, V., Riech, V., Rösch, H., Schäfer, P., Schulte, S., Sirocko, F., and Tahir, M.: Sampling the oxygen minimum zone off Pakistan: glacial-interglacial variations of anoxia and productivity (preliminary results, SONNE 90 cruise), Marine Geology, 125, 7-19, 1995.

Von Rad, U.: Physical oceanography during SONNE cruise SO90, PANGAEA, doi:10.1594/PANGAEA.805802, 2013.

Walker, M. J., Berkelhammer, M., Björck, S., Cwynar, L. C., Fisher, D. A., Long, A. J., Lowe, J. J., Newnham, R. M., Rasmussen, S. O., and Weiss, H.: Formal subdivision of the Holocene Series/Epoch: a Discussion Paper by a Working Group of INTIMATE (Integration of ice-core, marine and terrestrial records) and the Subcommission on Quaternary Stratigraphy (International Commission on Stratigraphy), Journal of Quaternary Science, 27, 649-659, 2012.

Wang, L., Sarnthein, M., Duplessy, J. C., Erlenkeuser, H., Jung, S., and Pflaumann, U.: Paleo sea surface salinities in the low-latitude Atlantic: The $\delta^{18}O$ record of *Globigerinoides ruber* (white), Paleoceanography, 10, 749-761, 1995.

Wanner, H., Beer, J., Bütikofer, J., Crowley, T. J., Cubasch, U., Flückiger, J., Goosse, H., Grosjean, M., Joos, F., Kaplan, J. O., Küttel, M., Müller, S. A., Prentice, C., Solomina, O., Stocker, T. F., Tarasov, P., Wagner, M., and Widmann, M.: Mid-to Late Holocene climate change: an overview, Quaternary Science Reviews, 27, 1791-1828, 2008.

Weatherall, P., Marks, K., Jakobsson, M., Schmitt, T., Tani, S., Arndt, J. E., Rovere, M., Chayes, D., Ferrini, V., and Wigley, R.: A new digital bathymetric model of the world's oceans, Earth and Space Science, 2, 331-345, 2015.

Weber, S.: Seeds of urbanism: palaeoethnobotany and the Indus Civilization, Antiquity, 73, 813-826, 1999.

Weber, S. A.: Archaeobotany at Harappa: indications for change, Indus ethnobiology: new perspectives from the field, 175-198, 2003.

Weber, S. A., Barela, T., and Lehman, H.: Ecological continuity: An explanation for agricultural diversity in the Indus Civilization and beyond, Man and Environment, 35, 62-75, 2010.

Weiss, H.: Global megadrought, societal collapse and resilience at 4.2-3.9 ka BP across the Mediterranean and West asia, Clim. Chang. Cult. Evol, PAGES Mag, 24, 62, 2016.

Wick, L., Lemcke, G., and Sturm, M.: Evidence of Lateglacial and Holocene climatic change and human impact in eastern Anatolia: high-resolution pollen, charcoal, isotopic and geochemical records from the laminated sediments of Lake Van, Turkey. The Holocene, 13, 665-675, 2003.

Wright, R. P.: The ancient Indus: urbanism, economy, and society, Cambridge University Press, Great Britain, 107, 2010.

Yadav, R. K., Kumar, K. R., and Rajeevan, M.: Characteristic features of winter precipitation and its variability over northwest India. J. Earth Syst. Sci., 121, 611-623, 2012.

Yu, W., Yang, Y. C., Savitsky, A., Alford, D., Brown, C., Wescoat, J., Debowicz, D., and Robinson, S.: The Indus basin of Pakistan: The impacts of climate risks on water and agriculture, The World Bank, 2013.

Zaric, S.: Planktic foraminiferal flux of sediment trap EAST-86/90_trap, PANGAEA, doi: 10.1594/PANGAEA.264508, 2005.

Zweng, M. M., Reagan, J. R., Antonov, J. I., Locarnini, R. A., Mishonov, A. V., Boyer, T. P., Garcia, H. E., Baranova, O. K., Johnson, D. R., Seidov, D., and Biddle, M. M.: World Ocean Atlas 2013, Volume 2: Salinity. Levitus, S. (Ed.), Mishonov, A. (Technical Ed.), NOAA Atlas NESDIS 74, 39, 2013.

Supplemental figures and tables

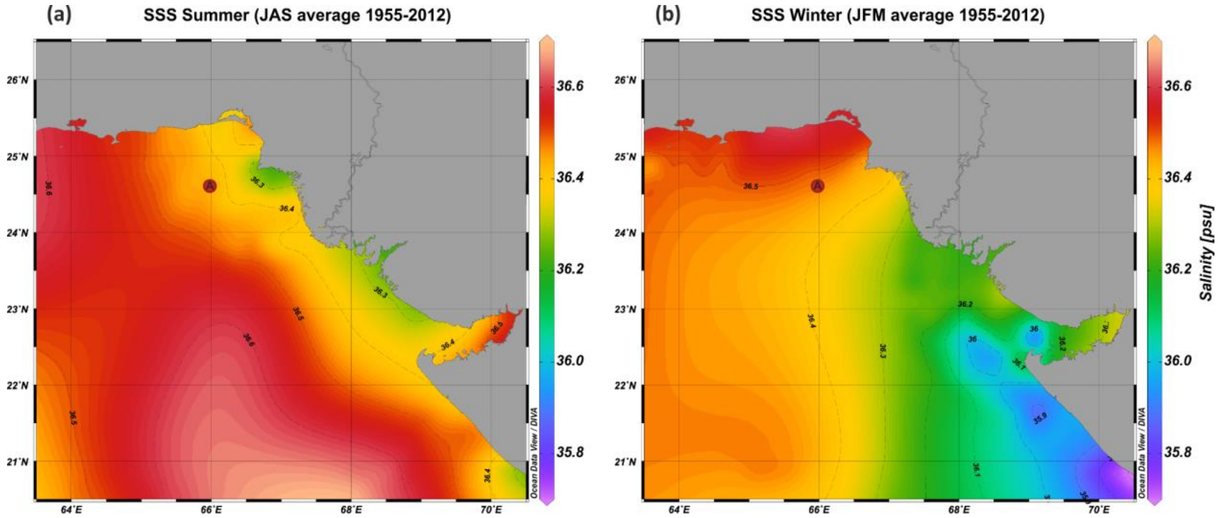

Figure S1. Mean surface salinity for 1955-2012, with data from the 2013 World Ocean Atlas (WOA) at 0.25° resolution (Zweng et al., 2013). Salinity contours are shown for **a.** summer (JAS) and **b.** winter (JFM). The Indus River is outlined. Note that over the time window of this dataset, modern Indus River discharge has been reduced by >50% due to barrages and irrigation (Ahmad et al., 2001). Plots created with Ocean Data Viewer (ODV).

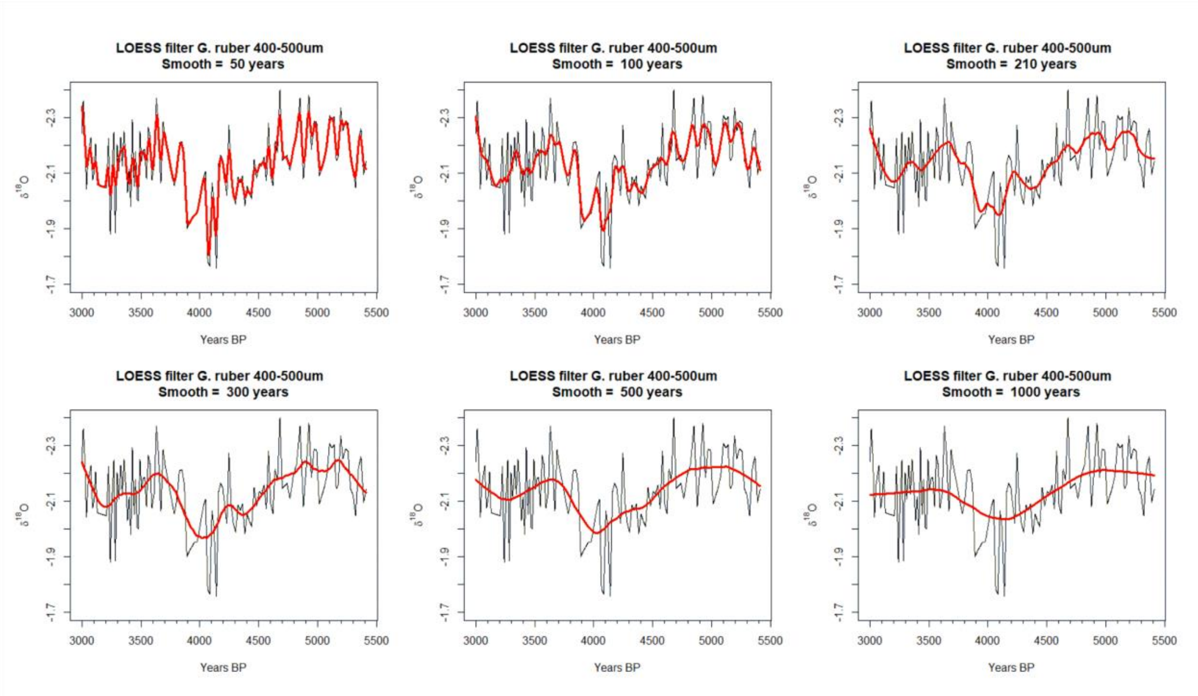

Figure S2. Comparison of loess smoothing windows of 50, 100, 210, 300, 500, and 1000 years for *G. ruber* in the 400-500µm fraction.

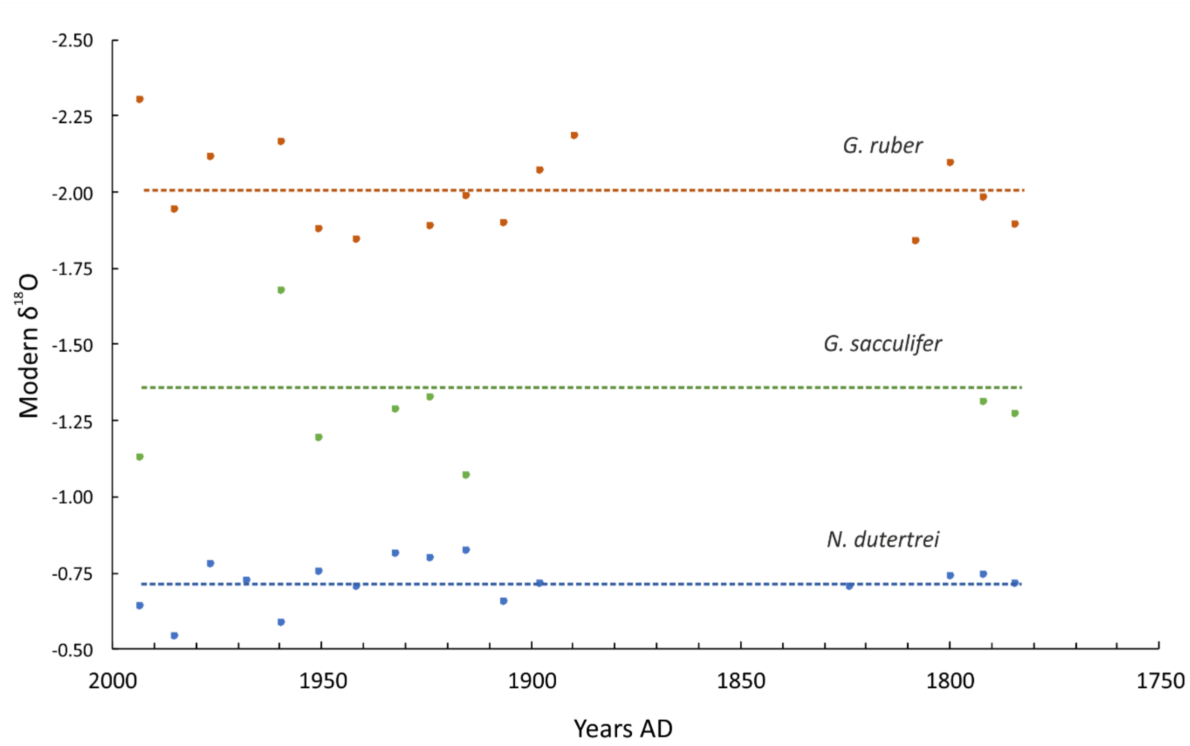

Figure S3. Modern $\delta^{18}O$ values of calcite, spanning approximately the last 200 years, measured from surface sediment samples for all three species at the size fractions 315-400µm. Averages values for the last 200 years (~1780-1993 AD) are compared to the period 5.4-3.0 ka BP: -2.01‰ (modern) and -1.90‰ (old) for *G. ruber* (orange), -1.28‰ (modern) and -1.31‰ (old) for *G. sacculifer* (green), and -0.72‰ (modern) and -0.76‰ (old) for *N. dutertrei* (blue).

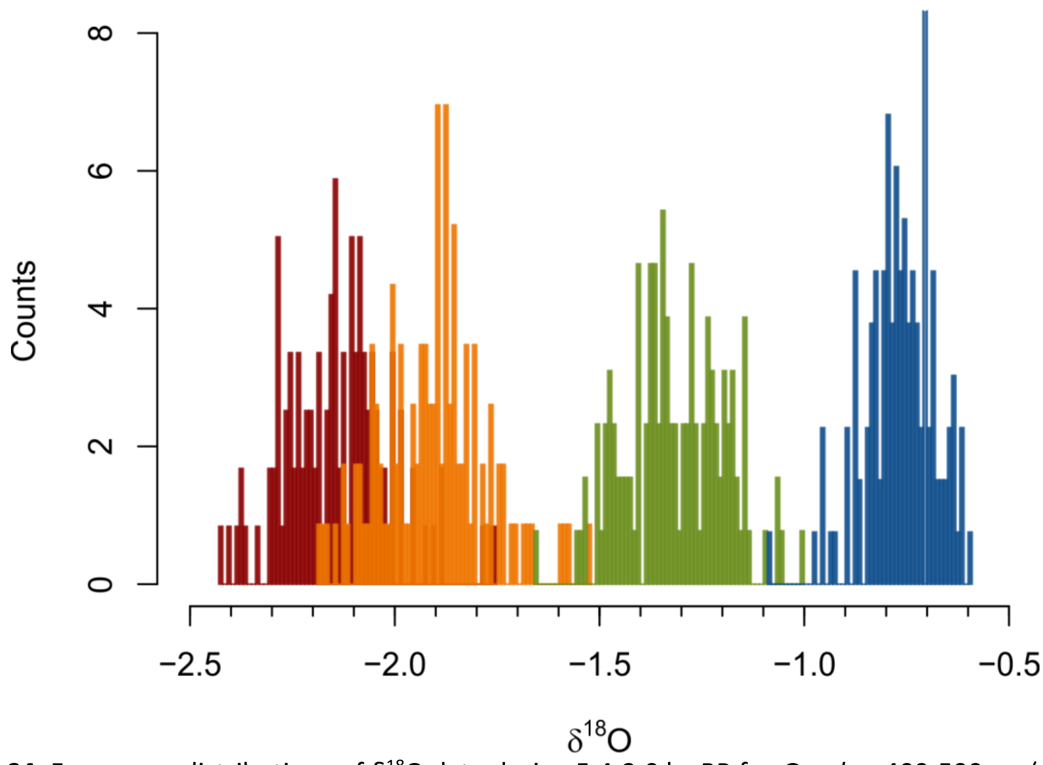

Figure S4. Frequency distributions of $\delta^{18}O$ data during 5.4-3.0 ka BP for *G. ruber* 400-500µm (red), *G. ruber* 315-400µm (orange), *G. sacculifer* 315-400µm (green), *N. dutertrei* 315-400µm (blue).

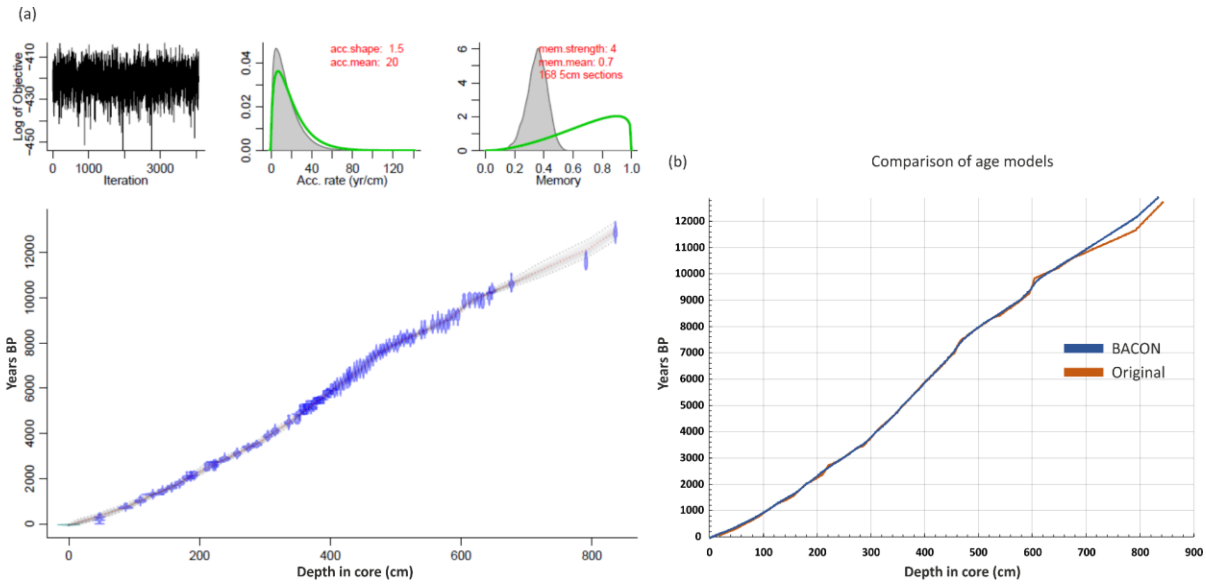

Figure S5. a. BACON age-depth model with calibrated dates shown in blue **b.** Age-depth model comparison with the original published age model from Staubwasser et al. (2003) (orange) and the new age model based on BACON software (blue).

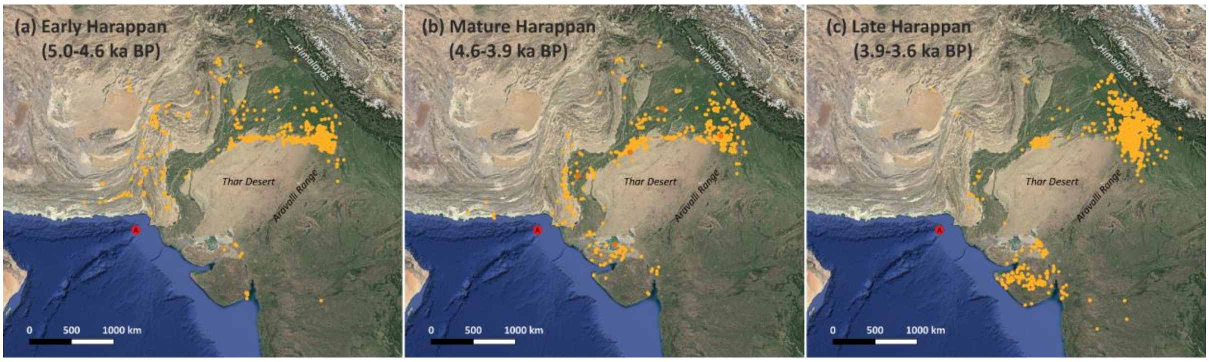

Figure S6. Indus site distributions (yellow points) during the **a.** Early Harappan (~5.0-4.6 ka BP), **b.** Mature Harappan (~4.6-3.9 ka BP), and **c.** Late Harappan (~3.9-3.6 ka BP). Orange sites show larger Harappan cities during the Mature Harappan period (Dholavira, Mohenjo Daro, Ganweriwala, Harappa, and Rakhigarhi from bottom to top), core 63KA shown by red circle, background terrain from Google Earth.

Table S1. Main statistical parameters of the $\delta^{18}O$ data.

	G. ruber 400-500µm	*G. ruber 315-400µm*	*G. sacculifer 315-400µm*	*N. dutertrei 315-400µm*
n	119	115	129	132
Minimum	-2.423	-2.190	-1.660	-1.090
Maximum	-1.752	-1.520	-1.000	-0.590
1st Quartile	-2.232	-1.995	-1.400	-0.810
3rd Quartile	-2.068	-1.830	-1.220	-0.700
Mean	-2.139	-1.901	-1.312	-0.761
Median	-2.144	-1.890	-1.320	-0.760
Sum	-254.58	-218.66	-169.26	-100.46
SE Mean	0.012	0.012	0.011	0.007
LCL Mean	-2.163	-1.926	-1.333	-0.776
UCL Mean	-2.116	-1.877	-1.291	-0.746
Variance	0.016	0.017	0.015	0.007
Stdev	0.128	0.131	0.122	0.085

Skewness	0.408	0.288	-0.011	-0.592
Kurtosis	0.511	0.174	-0.364	0.850

Table S2. Age-Model calibration with BACON software.

Depth (cm)	*^{14}C date*	*Error (±1σ)*	*Reservoir (years)*	*IntCal13 min age BP*	*IntCal13 max age BP*	*IntCal13 mean age BP*
surface	-	-	-	-	-	-43
47	790	30	565	267	309	288
87	1370	35	565	678	780	729
109.5	1665	30	565	952	1062	1007
128.5	1955	25	565	1283	1339	1311
143.5	2115	35	565	1369	1529	1449
157.5	2270	25	565	1552	1634	1593
169.5	2430	25	565	1728	1869	1799
180.5	2640	25	565	1988	2122	2055
186.5	2675	35	565	1993	2154	2074
191.5	2720	30	565	2044	2184	2114
211.5	3000	35	565	2356	2541	2449
221.5	3110	40	565	2491	2602	2547
224.5	3145	25	565	2708	2758	2733
238.5	3340	25	565	2836	2929	2883
257.5	3510	30	565	2999	3181	3090
274.5	3730	30	565	3343	3451	3397
287.5	3850	30	565	3450	3576	3513
304.5	4145	30	565	3828	3975	3902
315.5	4310	30	565	4062	4159	4111
336.5	4570	40	565	4408	4578	4493
349.5	4655	40	565	4512	4711	4612
353.5	4870	30	565	4832	4892	4862
357.5	5005	35	565	4952	5079	5016
360.5	4980	30	565	4868	5057	4963
363.5	5080	30	565	5050	5194	5122
366.5	5105	35	565	5053	5189	5121
370.5	5070	35	565	5046	5300	5173
374.5	5160	40	565	5372	5463	5418
378.5	5210	40	565	5303	5469	5386
381.5	5315	30	565	5460	5585	5523
385.5	5315	35	565	5453	5586	5520
389.5	5420	35	565	5580	5654	5617
395.5	5635	35	565	5741	5907	5824
398.5	5610	35	565	5713	5904	5809
402	5750	40	565	5891	6008	5950
406.5	5830	35	638	5899	6002	5951
410.5	5965	40	638	5994	6210	6102
415.5	5980	45	638	5997	6216	6107
420.5	6120	45	638	6201	6351	6276

425.5	6265	45	638	6311	6490	6401
428.5	6335	55	638	6395	6639	6517
430.5	6345	60	638	6396	6657	6527
436.5	6440	40	638	6495	6678	6587
440.5	6540	55	638	6627	6883	6755
445.5	6665	45	638	6773	6984	6879
450.5	6650	40	638	6749	6948	6849
455.5	6960	45	824	6912	7162	7037
460.5	7155	45	824	7166	7331	7249
465.5	7310	45	824	7308	7480	7394
470.5	7480	55	824	7438	7606	7522
476.5	7550	50	824	7551	7670	7611
480.5	7815	55	1011	7571	7743	7657
485.5	7920	70	1011	7617	7867	7742
490.5	8070	50	1011	7788	7976	7882
497.5	8130	55	1011	7837	8027	7932
502.5	8115	55	1011	7828	8020	7924
507.5	8400	60	1011	8148	8345	8247
512.5	8350	50	1011	8020	8218	8119
517.5	8490	50	1011	8194	8381	8288
522.5	8355	60	1011	8023	8312	8168
527.5	8510	60	1011	8194	8400	8297
539.5	8790	60	1118	8384	8563	8474
544.5	8880	55	1118	8425	8631	8528
556.5	9060	50	1118	8637	8986	8812
564.5	9120	70	1118	8636	9026	8831
570.5	9110	50	1118	8698	9007	8853
576.5	9060	50	1118	8637	8986	8812
581.5	9260	50	1118	8999	9153	9076
588.5	9390	50	1118	9119	9430	9275
595	9370	60	1118	9076	9419	9248
604.5	9570	50	781	9602	9952	9777
613	9660	70	781	9736	10194	9965
621.5	9670	50	781	9884	10189	10037
628	9650	70	781	9732	10188	9960
633	9570	80	781	9581	9963	9772
643	9770	70	781	9906	10251	10079
647.5	9920	60	781	10206	10436	10321
677	10160	60	781	10480	10752	10616
791	11145	50	1095	11325	11806	11566
836	12285	55	1300	12726	12995	12861